1 **Iron and silicon isotope behaviour accompanying weathering in Icelandic soils, and the**

2 **implications for iron export from peatlands**

3 Opfergelt S.[1,2], Williams H.M.[2,3], Cornelis J.T.[1,4], Guicharnaud R.A.[5,6], Georg R.B.[2,7], Siebert C.[2,8],

4 Gislason S.R.[5], Halliday A.N.[2], Burton K.W.[2,3]

5 [1] Earth and Life Institute, Université catholique de Louvain, Croix du Sud bte L7.05.10, 1348 Louvain-la-Neuve,
6 Belgium
7 [2] Department of Earth Sciences, University of Oxford, South Parks Road, Oxford, OX1 3AN, United Kingdom
8 [3] Department of Earth Sciences, Durham University, DH1 3LE, Durham, United Kingdom
9 [4] Gembloux AgroBio-Tech, Université de Liège, Av. Maréchal Juin 27, 5030 Gembloux, Belgium
10 [5] Institute of Earth Sciences, University of Iceland, Sturlugata 7, 101 Reykjavík, Iceland
11 [6] European Commission, Land Resource Management Unit, 21027 Ispra, Italy
12 [7] Trent University, Water Quality Centre, 1600 West Bank Dr., Peterborough, Ontario, Canada
13 [8] Geomar, Helmholtz Center for Ocean Research, Wischhofstrasse 1-3, 24146 Kiel, Germany
14 *Corresponding author : UCL/ELIE, Croix du Sud 2 bte L7.05.10 1348 Louvain-la-Neuve, Belgium, Tel: +32 10 47
15 36 22, Fax: +32 10 47 45 25, E-mail : sophie.opfergelt@uclouvain.be

16
17

18 **Abstract**
19

20 Incipient warming of peatlands at high latitudes is expected to modify soil drainage and hence the
21 redox conditions, which has implications for Fe export from soils. This study uses Fe isotopes to
22 assess the processes controlling Fe export in a range of Icelandic soils including peat soils derived
23 from the same parent basalt, where Fe isotope variations principally reflect differences in weathering
24 and drainage. In poorly weathered, well-drained soils (non-peat soils), the limited Fe isotope
25 fractionation in soil solutions relative to the bulk soil ($\Delta^{57}Fe_{solution-soil}$ = -0.11 ± 0.12 ‰) is attributed to
26 proton-promoted mineral dissolution. In the more weathered poorly drained soils (peat soils), the
27 soil solutions are usually lighter than the bulk soil ($\Delta^{57}Fe_{solution-soil}$ = -0.41 ± 0.32 ‰), which indicates
28 that Fe has been mobilised by reductive mineral dissolution and/or ligand-controlled dissolution. The
29 results highlight the presence of Fe-organic complexes in solution in anoxic conditions. An additional
30 constraint on soil weathering is provided by Si isotopes. The Si isotope composition of the soil
31 solutions relative to the soil ($\Delta^{30}Si_{solution-soil}$ = 0.92 ± 0.26 ‰) generally reflects the incorporation of
32 light Si isotopes in secondary aluminosilicates. Under anoxic conditions in peat soils, the largest Si
33 isotope fractionation in soil solutions relative to the bulk soil is observed ($\Delta^{30}Si_{solution-soil}$ = 1.63 ± 0.40
34 ‰) and attributed to the cumulative contribution of secondary clay minerals and amorphous silica
35 precipitation. Si supersaturation in solution with respect to amorphous silica is reached upon freezing
36 when Al availability to form aluminosilicates is limited by the affinity of Al for metal-organic
37 complexes. Therefore, the precipitation of amorphous silica in peat soils indirectly supports the
38 formation of metal-organic complexes in poorly drained soils. These observations highlight that in a
39 scenario of decreasing soil drainage with warming high latitude peatlands, Fe export from soils as Fe-
40 organic complexes will increase, which in turn has implications for Fe transport in rivers, and
41 ultimately the delivery of Fe to the oceans.

42 **Keywords:** basalt weathering, volcanic soil, Iceland, Fe isotopes, Si isotopes, Fe export, peat soil

43

44

1. INTRODUCTION

Iron in rivers ultimately originates from mineral weathering and export from soils. Rivers are a major source of Fe to the ocean, and Fe is an essential nutrient for marine primary production (Morel et al., 1991; Poulton and Raiswell 2002; Martin and Fitzwater, 1988; Boyd et al., 2000; Smetacek et al., 2012). Recent evidence suggests that peatlands play a pivotal role in the delivery of Fe to coastal waters, and the organic acids that originate in peat likely serve as the principal metal chelator for Fe transport in rivers (Krachler et al., 2005, 2010). The transport of Fe in these colloidal (<10 kD) metal-organic complexes is considered a major way for peat-derived riverine Fe to escape Fe oxyhydroxide precipitation and flocculation, and hence escape estuarine removal (Boyle et al., 1977; Krachler et al., 2005, 2010).

High latitude permafrost peatlands currently face dramatic changes in temperature (Westermann et al., 2015; Hecht et al., 2007), and the predicted 37% reduction of the permafrost extent by 2100 (IPCC 2013) is likely to result in significant changes in soil drainage. Although whether permafrost peatlands will become wetter or drier is still uncertain (e.g., Swindles et al., 2015). Changing freeze-thaw cycles and frequencies of seasonal anoxic soils is likely to impact redox-controlled process such as Fe mobilisation, and hence, Fe export from soils. In order to better predict the potential impact of warming peatlands at high latitudes on the Fe export from soils in these regions, a detailed understanding of processes controlling Fe behaviour in high latitude soils is required.

In soils, Fe is initially locked up in primary minerals. Through chemical weathering, Fe is mobilised by proton-promoted, ligand-controlled or reductive dissolution (e.g., Cornell and Schwertmann, 2003; Bonneville et al., 2004; Wiederhold et al., 2006; Melton et al., 2014). This mobilised Fe can reside in soils as secondary phyllosilicates, Fe oxyhydroxides and/or chelated as metal-organic complexes (e.g., Cornell and Schwertmann, 2003; Thompson et al., 2011), or be exported from soils. The evolution of Fe in secondary phases is a function of (i) soil drainage that affects redox processes, (ii) soil weathering degree that affects the mineral reserve and the solubility of minerals, and (iii) soil organic matter content that affects the amount and type of organic ligands (e.g., Schwertmann, 2008; Fritsch et al., 2009).

The stable iron isotope compositions of soils can be shifted from the composition of the parent material by the removal or addition of significant pools of fractionated Fe, providing a valuable approach to trace the processes controlling Fe mobilisation and export from soils (e.g., Fantle and De Paolo, 2004; Emmanuel et al., 2005; Wiederhold et al., 2007a; Thompson et al., 2007; Fekiacova et al., 2013; Mansfeldt et al., 2012; Liu et al., 2014; Schulz et al., 2016; Dauphas et al., 2017). More precisely, Fe isotopes in soils are sensitive to redox processes, to weathering processes and the formation of Fe-oxides, and to the formation of Fe-organic complexes. Light Fe isotopes are often enriched in soils containing secondary Fe phases (e.g., Wiederhold et al., 2007b; Kiczka et al., 2011; Guelke et al., 2010; Poitrasson et al., 2008; Yesavage et al., 2012; Liu et al., 2014 ; Fekiacova et al., 2017). This enrichment can be explained by the quantitative precipitation of light Fe-oxyhydroxides from light Fe isotopes preferentially released by proton-promoted mineral weathering (Chapman et al., 2009; Kiczka et al., 2010a), reductive mineral dissolution (e.g., Wiederhold et al., 2006, 2007a, 2007b), and ligand-controlled mineral dissolution (Brantley et al., 2001, 2004; Wiederhold et al., 2006, 2007b; Buss et al., 2010). In solution, there is an isotope fractionation between Fe(III) and Fe(II), with light isotopes accumulating in the Fe(II) (Johnson et al., 2002; Thompson et al., 2007;

87 Wiederhold et al., 2007a; Welch et al, 2003; Wu et al., 2011). The greater mobility of Fe(II) is a cause
88 of soil Fe isotope fractionation in anoxic soils, leaving a residual soil enriched in heavy Fe (e.g.,
89 Wiederhold et al., 2007a; Fekiacova et al., 2013; Akerman et al., 2014; Schuth et al., 2015). In the
90 presence of organic ligands, heavy Fe isotopes are favoured in Fe-organic complexes relative to
91 uncomplexed Fe in solution (Dideriksen et al., 2008; Morgan et al., 2010), potentially modifying the
92 Fe isotope fractionation induced by mineral dissolution.

93 Icelandic soils hosts high latitude soils, that range from poorly weathered, well drained, oxic soils to
94 more intensely weathered, poorly drained, peat-rich soils (i.e., anoxic, or seasonally anoxic) all
95 derived from a largely homogeneous basaltic bedrock. These soils therefore provide an ideal natural
96 laboratory to use Fe isotopes to investigate the controls on Fe export from soils under contrasting
97 soil drainage, soil weathering degree and soil organic matter content. The working hypothesis of this
98 study is that in poorly weathered well drained soils, a limited Fe isotope fractionation in solution
99 relative to the parent basalt is expected; by contrast, in the more weathered soils, given the poor
100 drainage and the high amount of soil organic carbon, Fe isotope fractionation in solution associated
101 with reductive dissolution, ligand-controlled dissolution, and leaching of Fe(II) is expected, and Fe-
102 organic complexation would modify the Fe isotope fractionation driven by mineral dissolution.

103 Additional constraint on the advance of weathering in soils can also be obtained from silicon isotopes
104 which are fractionated by weathering processes due to the preferential incorporation of light
105 isotopes in secondary aluminosilicates (e.g., Ziegler et al., 2005; Georg et al., 2009; Opfergelt et al.,
106 2010, 2012; Oelze et al., 2014). The formation of these secondary phases depends on Al availability,
107 which in organic-rich soils is limited due to the formation of Al-organic complexes (Parfitt, 2009;
108 Parfitt and Kimble, 1989; Mizota and van Reeuwijk, 1989). If the formation of secondary alumino-
109 silicates is limited, the Si concentration in solution may reach supersaturation with respect to
110 amorphous silica, for example upon freezing (Ping, 1988; Shoji and Masui, 1971). The precipitation of
111 amorphous silica fractionates Si isotopes (e.g., Li et al., 1995; Geilert et al., 2014, 2015; Roerdink et
112 al., 2015; Oelze et al., 2015), and would add to the Si isotope fractionation induced by clay formation.
113 Consequently, a second working hypothesis is that Si isotope fractionation in soils, if partly caused by
114 amorphous silica precipitation, indirectly provides a way to support the formation of metal-organic
115 complexes in soils.

116 This study tests these two hypotheses on Icelandic soils comparing organic-poor and organic-rich
117 soils derived from the same parental basalt. We report on Fe and Si isotope compositions of bulk
118 soils, secondary phases, and soil solutions with a detailed soil characterisation and information on
119 the distribution of Fe and Si.

120 **2. MATERIALS AND METHODS**

121   **2.1. Environmental setting**

122 The types of soils developed in Iceland are primarily determined by the drainage conditions and
123 aeolian volcanic ash inputs (Arnalds, 2004), which provide a source of fresh reactive material to the
124 developing soils. Soils in West Iceland receive lower amounts of aeolian ash deposition (~0.1 mm yr^{-1};
125 Sigfusson et al., 2008) relative to areas closer to the rift zones in South West Iceland (~2 mm yr^{-1};
126 Arnalds, 2004). In areas with vegetation cover, soils are classified as Andosols (~48 %; Haplic, Histic
127 and Gleyic Andosols), desert areas are dominated by poorly developed Vitric Andosols (~40 %) and

wetland areas by organic-rich Histosols (~1 %), with the rest of Iceland (~11%) being mainly covered by glaciers (Arnalds, 2004, 2008). The andic properties of the soils and the cold climate (mean summer temperature of 12 °C) are amongst the key factors that result in low rates of organic matter decomposition in Iceland (Guicharnaud, 2009). Oxidation is also impaired in poorly drained areas such that the accumulation of plant debris results in the progressive buildup of peat (Histic Andosol and Histosol).

The hydrology in Icelandic soils is affected by seasonal variability in runoff, which ranges from below 100 mm/season in the summer (June-July-August) to 200 - 400 mm/season in the winter (December-January-February) (Icelandic Meteorological Office; Crochet et al., 2007). The climate in the areas of the lowland soils (below 200 m altitude) is temperate, with a mean annual precipitation (MAP) of 1017 mm yr^{-1} and a mean annual temperature (MAT) of 4.6 °C. Due to the maritime winter climate of Iceland, the soils are exposed to more freeze-thaw cycles than many other subarctic regions (Orradottir et al., 2008; Arnalds, 2008). This leads to seasonal wet-dry cycles that influence water mobility in soils. Recently (post 1945), Icelandic inland wetland areas have been subject to a wide-scale draining subsidy driven by agriculture, mainly for hay-making (Arnalds et al., 2016). As a result of the installed ditch network or drainage trenches, inland wetlands are now strongly affected by drainage, especially in lowland areas, where up to 70% of the wetland areas are affected. Most of the poorly drained soils (Histic Andosol and Histosol) located in the lowland areas are, therefore, affected by drainage ditches. However, Histosols are still characterised by wetter conditions (more anoxic) than Histic Andosols (Arnalds, 2008).

2.2. Soil sampling and characterisation

Five typical Icelandic soil types (Histic Andosol, HA; Histosol, H; Haplic Andosol, BA; Gleyic Andosol, GA; Vitric Andosol, V) under grassland were sampled in September 2009 (location in Figure 1), including the parent basalt from the BA site, and the grass-type vegetation (hummocky grassland, bulk shoot part) was sampled in June 2010 from the HA site. The soil profiles were described following the World Reference Base for Soil Resources (IUSS, 2014; Table EA-1) and sampled by horizon. The profiles have been characterised previously for their Mg, Mo and Zn isotopic compositions (Opfergelt et al., 2014; Siebert et al., 2015; Opfergelt et al., 2017). The five soil profiles can be divided into two groups as a function of drainage: the freely drained soils V-BA-GA and the poorly drained soils HA-H. Profiles V, BA, and GA are characterised by a neutral pH and a low organic carbon content (pH 6.7 ± 0.7; 5.4 ± 2.9 % C; Table 1), in contrast to profiles HA and H which are acidic and organic rich soils (pH 4.8 ± 0.6; 21 ± 9 % C; Table 1; Opfergelt et al., 2014). The parent material is basaltic (main primary minerals: augite, Ca-rich plagioclase, magnetite, and glass). In volcanic soils, short-range ordered or poorly crystalline phases (i.e., aluminosilicates and Fe-oxides) are formed first (e.g., Rai and Kittrick, 1989; Thompson et al., 2011; Delmelle et al., 2015). With increasing time for soil development, the poorly crystalline phases transform to more crystalline minerals. Among the five soil profiles, the weathering degree increases in the following order: Basalt<V<BA<GA<H<HA (Opfergelt et al., 2014).

Iron was selectively extracted using dithionite-citrate-bicarbonate (DCB) (Fe_d; Mehra and Jackson, 1960), ammonium oxalate (Fe_o; Blakemore et al., 1981), and Na-pyrophosphate (Fe_p; Bascomb, 1968) and measured by ICP-AES. The analytical conditions for these extractions are provided in Table EA-2. The DCB-extractable Fe is used to provide an estimate of the content of free iron oxides in soils, i.e.,

170 poorly crystalline and crystalline Fe-oxides. The oxalate-extractable Fe is used as an indicator of

171 poorly crystalline Fe-oxides. The pyrophosphate-extractable Fe is used as an indicator of Fe-organic

172 complexes. These extractions are, however, to be considered with caution. Magnetite might be

173 partly dissolved by oxalate and contribute to Fe_o (e.g., Walker, 1983). The dithionite extraction is

174 usually considered to not dissolve magnetite, but some studies report magnetite dissolution with

175 DCB (e.g., Kostka and Luther, 1994; Henkel et al., 2016). The pyrophosphate is a dispersing agent and

176 Fe_p may include the contribution of Fe-oxide nanoparticulates in addition to the organically-bound Fe

177 (Jeanroy and Guillet, 1981), even if this contribution decreased by the centrifugation and filtration of

178 the extract (Table EA-1). These selective extractions are, therefore, not fully quantitative, but can,

179 nevertheless, be used as indicators of the evolution of the mineral phases as a function of the soil

180 development. The Fe_o/Fe_d ratio is used as a reflection of the relative proportion of short-range

181 ordered Fe oxyhydroxides (ferrihydrite) in the global pool of Fe-oxides. Within the total iron content

182 (Fe_t) in soils, the proportion of Fe contained in free Fe-oxides (Fe_d) is used as a weathering index (the

183 Fe_d/Fe_t ratio). The organic carbon released after dispersion by the pyrophosphate (C_p) was quantified

184 by combustion (Shimadzu TOC analyzer, detection limit < 2 mg L^{-1}) and is considered to provide an

185 indication of the amount of C that was included in metal-organic complexes (e.g. Cornu and Clozel,

186 2000; Cornu et al., 2008).

187 The oxalate-extractable Si (Si_o) was determined by ICP-AES to estimate the quantity of Si associated

188 with poorly crystalline aluminosilicates (allophane) as an indicator of the evolution of the mineral

189 phases in soils with weathering. The Si_o also includes the contribution from Si associated with poorly

190 crystalline Fe oxyhydroxides (ferrihydrite). The Si_o estimated this way is, however, to be considered

191 with caution because volcanic glass might also be partly dissolved using this protocol, particularly at

192 pH values below 6 (Oelkers and Gislason, 2001; Arnalds and Gislason, 2002; Wolff-Boenisch et al.,

193 2004). The DCB-extractable Si (Si_d) measured by ICP-AES can be used as an indicator of Si-bound to Fe

194 oxyhydroxides, but is also to be considered with caution given that partial dissolution of poorly-

195 crystalline silicate phases, such as allophane, by DCB may occur (e.g., Parfitt and Childs, 1988;

196 Borggaard, 1988; Ryan and Gschwend, 1991). Bulk soils (<2mm) were analysed by X-ray diffraction

197 (XRD, Bruker D8, Cu Kα), after oxalate extraction to remove poorly crystalline allophane and

198 ferrihydrite and H_2O_2 treatment to remove organic matter, to evaluate the presence of goethite and

199 amorphous silica.

200 **2.3. Soil solution and river water: sampling and characterisation**

201 Soil solutions, i.e., pore waters from the soil profiles (except V), were sampled in June 2010, using

202 macro rhizon soil water samplers (length 9 cm, diameter 4.5 mm, porosity 0.2 µm; Eijkelkamp®). The

203 soil horizons were fully saturated at the time of sampling in H-HA, but not in BA-GA. The rhizon

204 samplers were installed in soils for two weeks and collected every 24 hours to provide a bulk soil

205 solution (total volume of between 100 and 1500 ml), which was then acidified in 0.5% HNO_3 to

206 prevent oxidative precipitation. The Fe concentrations were measured by ICP-MS, and Si

207 concentrations by spectrophotometry (Opfergelt et al., 2014).

208 Three river water samples were collected in West Iceland in September 2009 (Figure 1). One river

209 sample (HA river) was collected next to the HA soil profile and the two other rivers (A3 and A4)

210 corresponding to localities A3 and A4 previously sampled to study the influence of weathering

211 processes on U and Li isotopes (Pogge von Strandmann et al., 2006), Mg isotopes (Pogge von

5

212   Strandmann et al., 2008), and Mo isotopes (Pearce et al., 2010) were sampled again. Water was
213   collected in pre-cleaned polypropylene bottles from the centre of the flow, and filtered within 24h
214   through 0.2 µm cellulose acetate filters. The temperature, pH, and electrical conductivity were
215   measured in the field. For river localities A3 and A4, the 0.2 µm filtered water was then ultrafiltered,
216   using a Sartorius cross-flow filter unit containing Sartocon polyethersulphone (PESU) slice cassettes,
217   in order to separate the colloidal fraction (> 10 kD) from the "truly" dissolved (< 10 kD) fraction. The
218   Fe concentration in the dissolved (< 0.2µm) and colloidal fraction (10 kD - 0.2 µm) was determined by
219   ICP-MS in 2 % HNO_3 (Open University, UK). The accuracy on the Fe concentration (± 7 %; < 0.01 µM
220   detection limit) was assessed using the water reference material SLRS-4 (measured Fe concentration
221   value of 110 ± 3 µg L^{-1} relative to certified value of 103 ± 5 µg L^{-1}; Yeghicheyan et al., 2001).

222   **2.4. Iron and silicon stable isotope measurements**

223   The Fe isotope compositions ($\delta^{57/54}$Fe, relative to the IRMM014 Fe standard) of the basalt (USGS
224   international rock standard BIR-1 which is an Iceland basalt), bulk soil samples (except for soil profile
225   V), selective extractions by dithionite-citrate-bicarbonate (Fe_d, excluding Fe bound in silicates, except
226   V; Guelke et al., 2010), soil solutions (except V), and the vegetation sample were analysed by MC-ICP-
227   MS (Thermo Neptune) at Durham University using standard Fe purification and mass spectrometry
228   procedures (Williams et al., 2012). Dissolution, Fe purification and isotope analyses were undertaken
229   using established procedures (Williams et al., 2014). Briefly, bulk soil samples and the vegetation
230   sample were first digested in aqua regia (3:1 HCl:HNO_3) and following a reflux and evaporation cycle,
231   were subsequently treated with concentrated HF:HNO_3 (10:1) in order to dissolve any detrital
232   material. Soil solutions and extractions were evaporated down. All samples were then oxidised with
233   several reflux (at 150°C) and evaporation (at 210°C) cycles of HNO_3 and H_2O_2 (repeatedly e.a. to
234   decompose the sulphide matrix from the dithionite reagent; e.g., Henkel et al., 2016), an important
235   step given that Fe isotope analysis of DCB extracts are challenging, after which they were converted
236   to 6M HCl form for anion column chemistry (AG1-X4, 200-400 mesh, chloride form). Iron yields were
237   quantitative and total procedural blanks were < 0.5 ng, which is negligible compared to the total
238   amount of Fe processed per soil sample or extraction (~ 20 µg). The analysed sample and standard
239   solutions comprised 2 ppm Fe in 0.1 M HNO_3. Sample and standard (IRMM-014) intensities (^{56}Fe and
240   ^{54}Fe) were matched to within 10 %. The standard ^{56}Fe beam intensity was in the range 2.5 to 3.5 × 10^{-}
241   ^{10} A. Measurements included collection of ^{57}Fe, ^{56}Fe and ^{54}Fe and ^{53}Cr to allow for correction of any
242   interference of ^{54}Cr on ^{54}Fe. We typically measured with a pseudo-high (peak-edge) resolution
243   (M/ΔM) of ~8500-9000. Errors are reported as the 2 standard deviations of replicate analyses. Mass
244   dependence, long-term reproducibility and accuracy were evaluated by analysis of an in-house FeCl
245   salt standard (δ^{57}Fe = -1.05 ± 0.07 ‰, 2SD, n=67) previously analysed in other studies (Williams et al.,
246   2014). The international rock standards BIR-1 (Icelandic basalt) and Nod-P1 (Pacific ferromanganese
247   nodule) were analysed over the course of this study. The mean Fe isotope compositions of these
248   standards are: δ^{57}Fe = 0.07 ± 0.04 ‰ (2SD, n = 4) for BIR-1, and -0.84 ± 0.02 ‰ for Nod-P1 (2SD, n =
249   7). These data are in excellent agreement with those reported previously (Millet et al., 2012; Weyer
250   et al., 2005; Williams et al., 2014).

251   The Si isotope compositions (δ^{30}Si, relative to the NBS-28 Si standard) of the parent basalt (from the
252   BA site; Opfergelt et al., 2014), bulk soil samples (all soils), clay fractions <2 µm (except V, recovered
253   after sonication, dispersion with Na^+-saturated resin of the <2mm fraction, separation from the
254   larger grain size by gravitational settling following the Stokes law, and flocculation of the clay

255 particles; Rouiller et al., 1972), and soil solutions were analysed by MC-ICP-MS at the University of
256 Oxford, UK, using standard Si purification and mass spectrometry procedures (Opfergelt et al., 2012).
257 Briefly, solid samples were ashed at 450 °C and dissolved by NaOH fusion at 720 °C in a silver
258 crucible. All samples were purified for Si isotope measurements using cation exchange resin (BioRad
259 AG50W-X12) (Georg et al., 2006). Silicon isotope compositions were determined on a Nu Plasma HR-
260 MC-ICP-MS in dry plasma mode in pseudo-high ("medium") resolution. Each sample was analysed 9
261 times, where each single δ-value (n) represents one sample run and two bracketed standard runs.
262 The mass dependence, accuracy and long-term reproducibility on $\delta^{30}Si$ were assessed over a period
263 of 12 months using the reference materials Diatomite (+1.25 ± 0.09 ‰, 2SD, n=132), Quartz Merck (-
264 0.05 ± 0.06 ‰, 2SD, n=45) and the USGS rock standard BHVO-2 (-0.26 ± 0.09 ‰, 2SD, n=124). These
265 values are in excellent agreement with those reported previously (Reynolds et al., 2007; Abraham et
266 al., 2008; Savage et al., 2010; Zambardi and Poitrasson, 2011).

3. RESULTS

268 All data are presented in Tables 1-3, in Figures 1-6 and in Figures EA-1 to EA-5 (for some parameters,
269 characterisation performed on a subset of samples).

3.1. Distribution of secondary phases in soils with weathering

271 Poorly crystalline aluminosilicates such as allophane are present in a higher amount in V-BA-GA than
272 in HA-H soils, and this is supported by a higher Si_o content in V-BA-GA (20.5 ± 6.0 g kg^{-1}) relative to
273 HA (10.6 ± 4.3 g kg^{-1}) and H (5.9 ± 3.0 g kg^{-1}; Table 1). The crystalline clay minerals that have been
274 identified are kaolinite and smectite (Opfergelt et al., 2014). The pool of free iron oxides (Fe_d/Fe_t)
275 increases with an increasing degree of weathering (Figure 2), and the proportion of short-range
276 ordered Fe-oxides in the global pool of Fe-oxides (Fe_o/Fe_d ratio) decreases with an increasing degree
277 of weathering (Figure EA-1a), suggesting that with increasing time for soil development poorly
278 crystalline Fe-oxyhydroxides, such as ferrihydrite, transform to more crystalline phases such as
279 goethite (shown by XRD; Figure EA-2). The proportion of Si_d is lower in V-BA-GA (Si_d/Si_t = 2.1 ± 0.5 %)
280 than in HA and H (HA = 4.8 ± 2.2 %; H = 3.3 ± 1.3 %; Table 1).

281 In addition to secondary aluminosilicates and Fe-oxides, Fe released from the weathering of primary
282 minerals may form metal-organic complexes. The amount of Fe_p is higher in HA-H soils (30.4 ± 17.6 g
283 kg^{-1}) than the V-BA-GA soils (4.1 ± 3.0 g kg^{-1}; Table 1), while the amounts of C_p are lower in V, BA and
284 GA soils (14.5 ± 8.0 g kg^{-1}) than in HA and H soils (49.6 ± 16.9 g kg^{-1}; Table 1). More specifically, the
285 proportion of Fe_p in the total soil Fe (Fe_p/Fe_t) is higher in H than in HA, and Fe_p correlates with the
286 amount of C_p in all soils (Figure EA-1b).

3.2. Iron isotope variations in soils, soil solutions and rivers

288 The poorly weathered soils (BA-GA) display relatively invariant Fe isotope compositions ($\delta^{57}Fe$ = 0.09
289 ± 0.08 ‰, 2SD, n=10; Table 1; Figure EA-3a) that are indistinguishable within error from the $\delta^{57}Fe$
290 value of the Iceland basalt BIR-1 (0.07 ± 0.04 ‰, 2SD), which is considered representative of the
291 parent material. At higher degrees of weathering and hence a higher amount of free Fe-oxides
292 (Figure 3a), the bulk soil Fe isotope compositions tend to deviate from the parent basalt composition,
293 with a trend towards lighter values in HA ($\delta^{57}Fe$ = -0.14 ± 0.33 ‰, 2SD, n=7) and heavier values in H
294 ($\delta^{57}Fe$ = 0.34 ± 0.26 ‰, 2SD, n=6). The pool of free Fe-oxides in soils (Fe_d) is characterised by $\delta^{57}Fe_{DCB}$

295   values that are generally lighter than the bulk soil (Figure 3b) and positively correlated with the δ^{57}Fe
296   of the bulk soil (R^2 = 0.56). Importantly, the bulk soil and the Fe_d pool of the least weathered soil BA
297   are characterised by δ^{57}Fe values (BA: δ^{57}Fe$_{bulk\ soil}$ = 0.13 ± 0.03 ‰, δ^{57}Fe$_{DCB}$ = 0.07 ± 0.09 ‰, 2SD) that
298   are within error of that of the Iceland basalt BIR-1 (0.07 ± 0.04 ‰, 2SD), as expected. These
299   observations provide further evidence that matrix effects do not compromise the Fe isotope analysis
300   of DCB extractions (Guelke et al., 2010).

301   The soil solutions are characterised by low Fe concentrations in BA-GA (0.02 ± 0.01 mg L^{-1}, n=10) and
302   HA (0.03 ± 0.01 mg L^{-1}, n=5) relative to H (from 0.06 to 25.07 mg L^{-1} Fe, with the highest
303   concentrations in H O4 (15.25 mg L^{-1} Fe) and H O6 (19.98 mg L^{-1} Fe; Table 2). The Fe isotope
304   compositions of the soil solutions are lighter than the bulk soils (Figure 3c) but not systematically
305   lighter than the Fe_d pool (Figure EA-3a). The δ^{57}Fe of the soil solutions are positively correlated with
306   the δ^{57}Fe of the bulk soil (R^2 = 0.55; in soil horizons for which δ^{57}Fe is available for bulk soils and soil
307   solutions: BA, HA, H). There is no difference between the δ^{57}Fe values in soil solutions relative to
308   Icelandic basalt (BIR-1) in BA-GA (0.02 ± 0.11 ‰, 2SD, n=4), a trend towards lighter values relative to
309   the basalt in HA soil solutions (δ^{57}Fe range from -1.36 to -0.08 ‰), while the heaviest δ^{57}Fe
310   compositions in soil solutions are found in H soil solutions (δ^{57}Fe range from -0.48 to +0.38 ‰; Figure
311   EA-3a). The lightest δ^{57}Fe in soil solutions are found in those characterised by the lowest pH (Table 1;
312   Figure EA-3b). The soil solutions with the highest Fe concentrations (H O4 and H O6) are
313   characterised by Fe isotope compositions of -0.48 ‰ and 0.14 ‰, respectively (Figure 3c). The
314   Icelandic grass collected is characterized by a δ^{57}Fe of -0.09 ± 0.03 ‰, 2SD (Table 1).

315   The river water samples collected in September 2009, A3 and A4, display similar temperature and pH
316   values (8.2 ± 1.4 °C and pH 8.2 ± 0.3; Table 3) and slightly higher conductivity values (57 ± 6 µS cm^{-1};
317   Table 3) relative to samples from the same rivers collected in September 2003 (average values for
318   localities A3 and A4: 10.7 ± 2.4 °C, pH 8.0 ± 0.1, conductivity 38 ± 4 µS cm^{-1}; Pogge von Strandmann et
319   al., 2006). The Fe concentration in the filtered fraction of those rivers (below 0.2 µm) ranges between
320   6 and 11.7 µg L^{-1} (Table 3), with between 26 and 56 % of Fe being colloidal (10 kD - 0.2 µm; Table 3).
321   In river sample A4, the Fe isotope composition of the filtered fraction (< 0.2 µm) is lighter (δ^{57}Fe = -
322   0.46 ± 0.07 ‰, 2SD) than the δ^{57}Fe value of the colloidal fraction (10 kD - 0.2 µm) (-0.14 ± 0.07 ‰,
323   2SD; Table 3).

324   **3.3. Silicon isotope variations in soils and soil solutions**

325   Bulk soil Si isotope compositions are generally lighter than that of the parent basalt (δ^{30}Si = -0.29 ±
326   0.06‰, 2SD) in V (-0.42 ± 0.05 ‰, 2SD, n=3) and in BA-GA (-0.61 ± 0.06 ‰, 2SD, n=11), and are the
327   lightest and most variable in HA (-0.91 ± 0.28 ‰, 2SD, n=7) and H (-0.74 ± 0.20 ‰, n=6, 2SD; Table 1;
328   Figure EA-4a). The δ^{30}Si values of the bulk soil samples become progressively lighter with greater
329   degree of weathering, as defined using the amount of free Fe-oxide (R^2 = 0.47; Figure 4a). The data
330   indicate that above 45 % clay content (< 2 µm; granulometric clay fraction with clay minerals and Fe-
331   oxides as the main mineral constituents), the Si isotope composition of the bulk soils becomes
332   systematically lighter (Table 1). The δ^{30}Si of the clay fractions are lighter than the δ^{30}Si of the bulk
333   soil, with a trend towards lighter δ^{30}Si $_{clay}$ with increasing weathering from BA-GA to HA (Figure 4b).

334   The Si concentrations in soil solutions in HA (20.03 ± 9.75 mg L^{-1}, n=5) are higher than in BA-GA (6.80
335   ± 3.21 mg L^{-1}, n=10), whereas H soil solutions display Si concentrations (14.25 ± 6.13 mg L^{-1}, n=5;
336   Table 2) that fall between those from BA-GA and HA but are not significantly different from each

337   other. The Si concentrations in soil solutions increase at lower pH (R^2 = 0.79; Table 1; Figure EA-4b).
338   The Si isotope compositions of soil solutions are heavier (+0.29 ± 0.37 ‰, 2SD, n=30; Table 2) than
339   the bulk soils (Figure 4c) and the Icelandic basalt (Figure EA-4a). There is no difference in δ^{30}Si
340   between the BA-GA and HA-H soil solutions (Table 2). The heaviest δ^{30}Si values in soil solutions are
341   found in the deep horizons of the H soil profile (H O4 + 0.88 ‰ and H O6 + 1.22 ‰; Figure 4c).

4. DISCUSSION

4.1. Iron isotope fractionation in soils

344   The δ^{57}Fe value of the Icelandic basalt used as representative of the parent material (BIR-1 = 0.07 ±
345   0.04 ‰, 2SD) is within the range of terrestrial igneous rocks (-0.1 to +0.15 ‰; Beard et al., 2003;
346   Figure 5a). The range of δ^{57}Fe observed in bulk Icelandic soils (-0.60 to +0.67 ‰) is within that of
347   existing iron isotope data for soils (recalculated where necessary from δ^{56}Fe to δ^{57}Fe using the mass-
348   dependent scaling factor of 1.5; e.g., from -0.9 to +1.4 ‰; Fantle and De Paolo, 2004; Emmanuel et
349   al., 2005; Thompson et al., 2007; Wiederhold et al., 2007a; Mansfeldt et al., 2012; Fekiacova et al.,
350   2013; Liu et al., 2014; Akerman et al., 2014; Liu et al., 2014; Schulz et al., 2016; Figure 5a), including
351   soils that formed in both oxic and anoxic weathering conditions. The δ^{57}Fe values of the free Fe oxide
352   pool (-1.07 to +0.25 ‰) are within the range of published values for pedogenic Fe-oxides (-1.07 to
353   +0.90 ‰; Wiederhold et al., 2007b; Kiczka et al., 2011; Guelke et al., 2010; Poitrasson et al., 2008;
354   Yesavage et al., 2012; Liu et al., 2014; Schuth and Mansfeldt 2015; Figure 5a).

355   Minimal δ^{57}Fe variations in the BA-GA bulk soils (0.09 ± 0.08 ‰, 2SD) relative to the parent basalt
356   (0.07 ± 0.04 ‰, 2SD) likely reflect the low degree of weathering of these soils, and the lower amount
357   of Fe-oxyhydroxides present compared to the HA-H soils (Figure 3a). This is supported by the "basalt-
358   like" δ^{57}Fe ratio in the volcanic ash horizon HA soil profile (HA redox, 67-83 cm depth = -0.05 ± 0.05
359   ‰, 2SD; Figure 3a; Table EA-1). In this volcanic ash layer, the heavier δ^{57}Fe value with respect to the
360   rest of the profile reflects the lower weathering degree of the material, i.e., a lower proportion of Fe-
361   oxyhydroxides (Figure 2). Aeolian deposition of volcanic ash at the top of the soils also contributes to
362   soil formation in Iceland (Arnalds, 2008). However, the influence of volcanic ash on soil Fe isotope
363   compositions is likely to be limited given that the aeolian contribution in the area of BA-GA-HA-H
364   soils in West Iceland are low (~0.1 mm yr^{-1}; Sigfusson et al., 2008) when compared to areas closer to
365   the rift zones in South West Iceland (~2 mm yr^{-1}; Arnalds, 2004).

366   The δ^{57}Fe values in HA bulk soils are heavier than the basalt at the surface and lighter than the basalt
367   below 25 cm depth (Figure EA-3a). The poorly drained conditions of this profile are likely to favour
368   the release of isotopically light Fe(II) under anoxic conditions, followed by the quantitative
369   precipitation of Fe-oxides during fluctuating oxic conditions (e.g., Fekiacova et al., 2013; Yesavage et
370   al., 2016) resulting in the enrichment of light Fe isotopes in pedogenic oxides in these soils
371   (Wiederhold et al., 2007a; Guelke et al., 2010; Kiczka et al., 2011). This hypothesis is supported by
372   the lighter δ^{57}Fe$_{DCB}$ composition of the Fe$_d$ pool relative to the bulk soils (Figure 3b) indicating a
373   preferential retention of light Fe isotopes in Fe-oxides. The fluctuations of oxic-anoxic conditions are
374   generated by frequent seasonal freeze-thaw cycles (Orradottir et al., 2008), and these fluctuations
375   occur more regularly in HA than H (Arnalds, 2008), and are amplified by drainage ditches in wetlands
376   (Arnalds et al., 2016). In addition, the presence of Fe-organic complexes may contribute to the Fe
377   isotope variability in the HA profile (δ^{57}Fe = -0.14 ± 0.33 ‰, 2SD), and lead to the heavier δ^{57}Fe
378   relative to the basalt observed above 25 cm. Iron-organic ligand complexation has been

379 experimentally shown to favour heavy Fe isotopes (Dideriksen et al., 2008; Morgan et al., 2010), as
380 predicted by the isotope fractionation theory for a stronger bonding environment (Schauble, 2004).
381 The correlation between Fe_p/Fe_t and C_p (Figure EA-1b) supports the presence of Fe-organic
382 complexes in both HA and H soils. The formation of metal-organic complexes is favoured by the
383 higher amounts of organic carbon available in the HA-H soils relative to the BA-GA soils (Table 1), and
384 by the lower pH in the HA-H soils than in BA-GA soils (Table 1) enhancing the rate of glass dissolution
385 (Oelkers and Gislason, 2001) and thereby creating a larger dissolved Fe pool.

386 The $\delta^{57}Fe$ values in the H bulk soils are heavier than the basalt suggesting the loss of light Fe isotopes
387 from this soil. The poorly drained conditions (mainly anoxic) of this profile are likely to favour the
388 release of isotopically light Fe(II) by reductive dissolution. The reduction of Fe is known to lead to a
389 fractionation of Fe isotopes, with Fe(II) being isotopically lighter than Fe(III) (Thompson et al., 2007;
390 Wiederhold et al., 2007a; Welch et al, 2003; Wu et al., 2011), and the greater mobility of Fe(II) in
391 aqueous solutions during weathering and soil development progressively depletes the soil in light Fe
392 isotopes, and leaves the residual material enriched in heavy Fe (e.g., Wiederhold et al., 2007a;
393 Fekiacova et al., 2013; Akerman et al., 2014; Schuth et al., 2015). The existence of drainage ditches
394 in wetlands (Arnalds et al., 2016) can potentially expose the H soil profile to oxic conditions for short
395 periods of time, which could explain the presence of secondary Fe-oxides in this soil and the range of
396 Fe isotope variability of the bulk soils ($\delta^{57}Fe$ = 0.34 ± 0.26 ‰, 2SD). The variable $\delta^{57}Fe$ isotope
397 composition of the Fe_d pool is similar to or heavier than the bulk soil in the H profile (except one
398 lighter value; Figure 3b) and this suggests that the quantitative precipitation of Fe-oxides has
399 occurred following a loss of light Fe isotopes. In addition, the formation and quantitative
400 accumulation of Fe-organic complexes may contribute to the Fe isotope variability in the H profile.
401 This process is likely to occur to a greater extent in H than in HA, given the anoxic conditions
402 releasing Fe by reductive dissolution (highest Fe concentration in soil solution in H; Table 1), resulting
403 in the higher proportion of Fe_p in the H soil than in the HA soil (higher Fe_p/Fe_t; Figure EA-1b).

404 Iron recycling by vegetation, including plant Fe uptake and decomposition of organic matter, is likely
405 to contribute to the Fe isotope variability in soils, especially in organic-rich soils such as HA-H. The
406 $\delta^{57}Fe$ value in plant available from the HA site (Icelandic grass: $\delta^{57}Fe$ = -0.09 ± 0.03 ‰, 2SD; Table 1)
407 is isotopically similar or heavier than the HA soil solution (Table 2). However, the Fe isotope
408 fractionation in plants is still debated (e.g., Guelke-Stelling and von Blanckenburg, 2012; Caldelas and
409 Weiss 2017) as it may depend on different parameters such as the plant Fe acquisition strategy
410 (Marschner and Römheld, 1994; Guelke and von Blanckenburg, 2007) or the nutrient status of the
411 soils (Kiczka et al., 2010b). It is therefore difficult to predict if heavier or lighter Fe isotopes are
412 preferentially taken up by vegetation at the studied field sites based on the available data. The Fe
413 concentrations of vegetation from the BA-GA-HA-H soils ranges from 0.2 to 0.4 g kg^{-1} (Opfergelt et
414 al., 2014), in good agreement with reported values for Fe concentrations in Icelandic grass 0.1 to 1.4
415 g kg^{-1} (e.g., Johannesson et al., 2007). Taking a biomass production of ~2 t ha^{-1} yr^{-1} (Opfergelt et al.,
416 2014), the Fe uptake by vegetation ranges from 0.4 to 0.9 kg ha^{-1} yr^{-1}. Relative to the total soil Fe
417 reservoir (between 134 and 338 kg ha^{-1} in the top 40 cm of the soil profile, calculated for each profile
418 from the total Fe concentration in soil horizons above 40 cm in Table 1, and the bulk density of soil
419 horizons provided in Opfergelt et al., 2014), the annual Fe uptake in vegetation represents 0.3% to
420 0.6% of the soil Fe reservoir. Therefore, although Fe recycling by vegetation may contribute to the
421 overall Fe isotope variability in bulk soils, this contribution is limited relative to the other processes
422 previously discussed.

4.2. Controls on Fe in soil solutions

The δ^{57}Fe values of the soil solutions, generally lighter than their corresponding bulk soils (Figure 3c), indicate the preferential release of light Fe isotopes in the dissolved pool relative to the solid pool, or a preferential removal of heavy Fe isotopes from the soil solution. The limited Fe isotope fractionation in soil solutions relative to the bulk soil in BA-GA (Δ^{57}Fe$_{solution-soil}$ = -0.11 ± 0.12 ‰; Figure 6) reflects the limited Fe isotope fractionation in poorly weathered soils (Figure EA-3a): the trend to release light Fe isotopes likely reflects primary mineral weathering by proton-promoted dissolution (Chapman et al., 2009; Kiczka et al., 2010a).

The δ^{57}Fe values in the HA soil solutions are lighter relative to the bulk soil except for HA Bw1 where the solution is heavier (Δ^{57}Fe$_{solution-soil}$ in HA = -0.76 to + 0.25 ‰; Figure 6). The dissolution of glass is favoured given the low pH of the HA soil (as supported by the high Si concentration in solution; Figure EA-4b). Given that the HA soil is organic-rich, ligand-controlled mineral dissolution is likely to contribute to the release of Fe, favouring light Fe isotopes. In this soil, characterised by fluctuating oxic-anoxic conditions, reductive dissolution is likely to occur and release light Fe isotopes during periods of anoxia. Iron reduction may mobilize colloidal Fe-organic complexes and Fe-oxides from the soil (Buettner et al., 2014; Thompson et al., 2011). Mobilisation of colloidal Fe-oxides to soil solutions can provide some explanation of the lighter δ^{57}Fe in soil solutions relative to bulk soils, given that the δ^{57}Fe$_{DCB}$ is similar to or lighter than the δ^{57}Fe of bulk soils (Figure 3b). Mobilisation of colloidal Fe-organic complexes, e.g., from the surface horizon HA A1 and horizon A2, may contribute to the heavier δ^{57}Fe values in the soil solution of the horizon HA Bw1, given that organic-Fe complexation favours heavy Fe isotopes (Dideriksen et al., 2008; Morgan et al., 2010).

The δ^{57}Fe values in H soil solutions are lighter than the bulk soil (Δ^{57}Fe$_{solution-soil}$ = -0.45 ± 0.24 ‰; Figure 6), but not as light as the HA soil solutions relative to the bulk soil (Δ^{57}Fe$_{solution-soil}$ up to -0.76 ‰ in HA). The poorly drained conditions (mainly anoxic) in H soil favour reductive dissolution and the release of isotopically light Fe(II) (Thompson et al., 2007; Wiederhold et al., 2007a; Welch et al, 2003; Wu et al., 2011), and this is supported by the highest Fe concentrations in solution in H, especially at depth (below 52 cm depth, in H O4 and H O6, 15.25 and 19.98 mg L^{-1} Fe, respectively), relative to the other soil profiles (BA-GA: 0.02 ± 0.01 mg L^{-1}, n=10; HA: 0.03 ± 0.01 mg L^{-1}, n=5; Table 2). In addition, as for the soil profile HA, ligand-controlled mineral dissolution may also contribute to the release of light Fe isotopes in the H soil solutions, and Fe reduction may mobilize colloidal Fe as Fe-organic complexes or Fe-oxides (Buettner et al., 2014; Thompson et al., 2011) and contribute to the δ^{57}Fe variability in solutions. The soil solutions of H O4 and H O6 are dominated by dissolved Fe(II) released under anoxic conditions, as supported by the high Fe concentrations in these soil solutions. Interestingly, the H O6 soil solution, which is characterised by a higher Fe concentration (19.9 mg L^{-1} Fe), is isotopically heavier (0.14 ‰) than the soil solution of H O4 (-0.48 ‰; Figure 3c) which has a lower Fe concentration (15.2 mg L^{-1} Fe; Table 2). These observations suggest that the δ^{57}Fe in H soil solutions is not only driven by light Fe(II) (Johnson et al., 2008), but modified towards heavier δ^{57}Fe values by the preferential retention of heavy Fe isotopes in solution, relative to the more mobile and isotopically lighter Fe(II). The formation of Fe-organic complexes in solution is expected to favour the incorporation of heavy Fe isotopes (Dideriksen et al., 2008; Morgan et al., 2010). The formation of Fe-organic complexes in the H soil profile is consistent with the higher Fe$_p$/Fe$_t$ of the bulk H soil relative to the other soils (Figure EA-1b). These observations point to a contribution from colloidal Fe-organic complexes in soil solutions from the H soil profile, i.e., characterised by more anoxic

466 conditions (Figure 6). This is consistent with observations in a tropical setting in Brazil, where Fe is
467 leached from soils as Fe-organic complexes in lowlands characterised by poorly drained
468 (waterlogged) organic-rich environments involving Fe reductive dissolution in anoxia (Chauvel et al.,
469 1987; Lucas et al., 1987; Fritsch et al., 2011).

470 **4.3. Silicon isotope fractionation in soils**

471 The δ^{30}Si isotope composition of the parent basalt (-0.29 ± 0.06 ‰, 2SD) is consistent with previously
472 published values for basalts (BHVO-2 = -0.31 ± 0.06 ‰, 2SD; e.g., Abraham et al., 2008), and with the
473 overall rather uniform δ^{30}Si composition of terrestrial basalts (Savage et al., 2010; Figure 5b). The Si
474 isotope composition of bulk soils (ranging from -1.32 to -0.38 ‰) and clay fractions (ranging from -
475 2.04 to -0.63‰) are within the range of previously reported Si isotope values for such materials
476 (review in Opfergelt and Delmelle, 2012; Frings et al., 2016; Poitrasson, 2017; Figure 5b). The
477 evolution of the Si isotope compositions of soils and clay fractions towards lighter δ^{30}Si values with
478 increasing degree of weathering (Figure 4a and 4b) is consistent with a preferential incorporation of
479 light Si isotopes in secondary weathering phases, resulting in light δ^{30}Si in soils and clay fractions
480 relative to the parental basalt (e.g., Ziegler et al., 2005; Georg et al., 2009; Opfergelt and Delmelle,
481 2012). The relationship between the weathering degree and the bulk soil δ^{30}Si is also supported by
482 the heavier δ^{30}Si of the HA horizon corresponding to a volcanic ash layer (HA redox, 67-83 cm depth =
483 -0.42 ± 0.14 ‰, 2SD) close to the basalt δ^{30}Si value, and to the heavier δ^{30}Si of the H O4 horizon
484 located underneath a volcanic tephra layer (H tephra 40-52 cm; Table EA-1) and potentially including
485 a basaltic contribution (H O4 = -0.47 ± 0.08 ‰, 2SD) (Figure 4a).

486 The presence of Fe-oxides in the secondary clay fractions may contribute to the light Si isotope
487 composition of those clay fractions, due to the Si adsorption onto Fe-oxides (Jones and Handreck,
488 1983; Hiemstra et al., 2007; Swedlund and Webster, 1999) favouring isotopically light Si (Delstanche
489 et al., 2009; Opfergelt et al., 2009). However, the Si_d/Si_t ratio, that can be used as a relative indicator
490 of the contribution of Si adsorbed onto Fe-oxides to the total Si content in soils, suggests that the
491 proportion of Si_d in Icelandic soils is limited (Si_d/Si_t: BA-GA = 2.2 ± 0.5 %; HA = 4.8 ± 2.2 %; H = 5.2 ±
492 3.3 %; Table 1). Even if the Si_d/Si_t ratio is two times higher in HA than in BA-GA, the proportion of Si
493 adsorbed is below 8 %, which is limited relative to Si mass in aluminosilicates. Consequently, the
494 contribution of light Si isotopes adsorbed onto Fe-oxides to the observed isotope difference between
495 $\delta^{30}Si_{clay}$ in HA (-1.67 ± 0.35 ‰, 2SD) and in BA-GA (-0.98 ± 0.24 ‰, 2SD; Table 1) is probably limited.

496 In secondary aluminosilicates, there is an evolution from poorly crystalline aluminosilicates such as
497 allophane forming in poorly weathered soils V-BA-GA (as supported by higher Si_o content than in HA-
498 H; Table 1), towards crystalline aluminosilicates such as kaolinite in more weathered soils HA-H. That
499 evolution is generally accompanied by a decrease of the δ^{30}Si value of the clay minerals (e.g., Ziegler
500 et al., 2005; Opfergelt et al., 2012; Cornelis et al., 2014), in good agreement with the decrease in
501 $\delta^{30}Si_{clay}$ from BA-GA to HA (Figure 3b).

502 In organic-rich soils, such as HA-H (Table 1), the affinity of Al for organic ligands at relatively low pH
503 limits Al availability for the formation of allophane (Parfitt, 2009; Parfitt and Kimble, 1989; Mizota
504 and van Reeuwijk, 1989). These conditions, combined with the enhanced dissolution of glass at lower
505 pH (Oelkers and Gislason, 2001), favour the increase of the Si concentration in solution (Figure EA-
506 4b). During periods of freezing, Si supersaturation with respect to amorphous silica may be reached,
507 leading to amorphous silica precipitation (Ping, 1988; Shoji and Masui, 1971; Dietzel, 2005). The

occurrence of amorphous silica is confirmed by XRD for the HA-H soils and is not observed in the V-BA-GA soils (Figure EA-2). The light isotopes of Si are known to be preferentially incorporated into amorphous Si (e.g., Li et al., 1995; Geilert et al., 2014, 2015; Roerdink et al., 2015; Oelze et al., 2015), which may contribute to the lighter Si isotope compositions of the HA and H bulk soils relative to the V-BA-GA soils (Figure 4a). A contribution from phytoliths to the fraction of amorphous Si in soils cannot be ruled out (McKeague and Cline, 1963), but is unlikely to represent the only contribution to amorphous silica. To be detected by XRD, an amorphous phase needs to represent ~30% of the sample (e.g., Paque et al., 2016). Taking the Si content in plants (25 g kg^{-1}; Opfergelt et al., 2014) and the amount of organic carbon in HA and H soils (between 18 and 42 %; Table 1), a minimum Si contribution from organic matter in soils would be ~1 % (considering a low organic matter decomposition), and that contribution alone would not be detected by XRD. The presence of phytoliths may contribute to the Si isotope variability in bulk soils but is unlikely to explain the lighter δ^{30}Si in HA-H soils relative to the other soils because plants preferentially incorporate the light Si isotopes (e.g., Opfergelt and Delmelle, 2012 and references therein) from soil solutions that are heavier than the bulk soil (Figure 4c). The presence of amorphous silica in HA-H and not in V-BA-GA supports the limited availability of Al to form alumino-silicates in HA-H relative to V-BA-GA, and provides indirect support for the formation of metal-organic complexes in HA-H, as suggested in section 4.2. The formation of metal-organic complexes involving Al in HA-H is confirmed by the higher proportion of pyrophosphate extractable Al (Al$_p$/Al$_t$, used to estimate metal complexes with organic ligands; Figure EA-1c) in HA-H than in BA-GA.

Heavier δ^{30}Si compositions in soil solutions (ranging from -0.19 to +1.22 ‰ in BA-GA-HA-H) relative to the basalt result from the preferential incorporation of light Si isotopes in secondary weathering phases (e.g., Ziegler et al., 2005; Georg et al., 2009; Opfergelt and Delmelle, 2012; Figure 5b). The Si isotope difference between the soil and the soil solution is within the same range in BA-GA and HA-H (Δ^{30}Si$_{solution-soil}$ = 0.92 ± 0.26 ‰) except in H soil profile below 50 cm where the soil solutions are heavier than any other soil solutions (for H O4 and H O6 solutions: Δ^{30}Si$_{solution-soil}$ = 1.63 ± 0.40 ‰; Figure 6; Figure 4c; Figure EA-4a). These data do not suggest a contribution from the dissolution of secondary minerals in HA-H organic rich-soils more acidic, as it would release light Si isotopes in solution (Cornelis et al., 2010; Steinhoefel et al., 2017). No specific process is reported to release of heavy Si isotopes in solution. Instead, successive mineral precipitation with the preferential incorporation of light Si isotopes may lead to a larger Si isotope fractionation between the soil and the soil solution. Successive precipitation of amorphous Si and clay minerals has been suggested in HA-H and not in BA-GA (Opfergelt et al., 2011). The heavier δ^{30}Si in H solutions relative to other soil solutions support that the precipitation of amorphous silica occurs in addition to the formation of secondary clay minerals. This is consistent with a limited availability of Al in H when metal-organic complexes are formed, as highlighted based on Fe isotopes (section 4.2; Figure EA-5a and 5b).

4.4. Implications for the Fe export to rivers

Based on the present study, it can be anticipated that if warming peatland at high latitudes (IPCC, 2013; Romanovsky et al., 2010) decreases soil drainage and leads to more anoxic soils, Fe export from soils as Fe-organic complexes will increase. Although beyond the scope of the present study, the potential implications for Fe in rivers can be considered based on the few Fe isotope compositions measured for Icelandic rivers from the catchment areas in which the soil profiles are located in (Table 3). The riverine Fe isotope compositions of the dissolved fraction (< 0.2 μm; δ^{57}Fe = -

551 0.55 ± 0.30 ‰, 2SD, n=3) are within the range of δ^{57}Fe values reported for the dissolved fraction of
552 other rivers (e.g., -1 to 0 ‰; Bergquist and Boyle, 2006; Mulholland et al., 2015; Figure 5a). The
553 dissolved Fe fraction of rivers (< 0.2 μm) includes truly dissolved Fe (<10 kD) and a range of colloidal
554 Fe (10 kD - 0.2 μm). The colloidal fraction of the A4 river locality (10 kD - 0.2 μm) is heavier (-0.14 ±
555 0.07 ‰, 2SD) than the corresponding dissolved fraction (< 0.2 μm; -0.46 ± 0.07 ‰, 2SD). Based on an
556 isotope mass balance calculation where 26 % of Fe has been measured in the colloidal fraction (Table
557 3), the δ^{57}Fe value of the truly dissolved Fe is -0.57 ‰, suggesting that the colloidal riverine Fe
558 fraction represents an isotopically heavier Fe carrier than the truly dissolved Fe. This observation is
559 consistent with the heavier δ^{57}Fe values reported for river colloids (Ingri et al., 2006; Ilina et al., 2013;
560 Akerman et al., 2014; Escoube et al., 2015; Mulholland et al., 2015; Figure 5a) relative to the
561 dissolved fraction of global rivers (e.g., Bergquist and Boyle, 2006).

562 The heavier δ^{57}Fe value of the colloidal fraction (10 kD - 0.2 μm) relative to the dissolved fraction (<
563 0.2 μm) of a local Icelandic river may reflect a contribution from colloidal Fe originating in soils.
564 Colloidal Fe exported from soils may be present as Fe oxyhydroxide nanoparticulates and/or Fe-
565 organic complexes (Thompson et al., 2011). In the context of organic-rich soils, the contribution of
566 Fe-organic complexes transported from soils (Chauvel et al., 1987; Lucas et al., 1987; Fritsch et al.,
567 2009, 2011) to rivers is thought to explain the heavy δ^{57}Fe ratio of the dissolved fraction of the Rio
568 Negro river relative to the dissolved fraction of the Amazon river, Brazil (Bergquist and Boyle, 2006;
569 dos Santos Pinheiro et al., 2014). In Iceland, the available δ^{57}Fe data for H soil solutions suggests that
570 the release of colloidal Fe from Histosols may contribute to the colloidal heavy δ^{57}Fe of rivers
571 draining peat soils. Further study is required to quantify the contribution from Fe oxyhydroxides
572 nanoparticules and/or Fe-organic complexes to the colloids exported from soils to rivers, and hence
573 the impact for Fe transport in rivers.

574 **5. CONCLUSIONS**

575 The Fe isotope composition in Icelandic soils provides important insights into the processes
576 controlling Fe export from high latitude soils as function of weathering and drainage (Figure 6).
577 During early weathering stages, well-drained soils do not generate any significant δ^{57}Fe isotope
578 variability in the bulk soils (0.09 ± 0.08 ‰, 2SD) relative to the δ^{57}Fe composition of the parent basalt
579 (0.07 ± 0.04 ‰, 2SD). In contrast, in poorly drained soils that have experienced a higher degree of
580 weathering, light Fe isotopes are released in solution by reductive or ligand-controlled mineral
581 dissolution. The Fe released is either quantitatively precipitated in Fe-oxides, where the fluctuating
582 redox conditions can account for the lighter δ^{57}Fe in soils (-0.14 ± 0.33 ‰, 2SD) than in the basalt and
583 increasingly lighter δ^{57}Fe in soils with increasing amount of Fe-oxides, or else leached from soils
584 under anoxic conditions leaving heavier δ^{57}Fe in soils (0.34 ± 0.26 ‰, 2SD) than in the basalt. In soil
585 solutions, a limited Fe isotope fractionation in poorly weathered well-drained soils (Δ^{57}Fe$_{\text{solution-soil}}$ = -
586 0.11 ± 0.12 ‰) reflects proton-promoted mineral dissolution (Figure 6). Larger Fe isotope
587 fractionation in more weathered poorly drained soils (Δ^{57}Fe$_{\text{solution-soil}}$ = -0.41 ± 0.32 ‰) reflects the
588 presence of Fe mobilised by reductive mineral dissolution and ligand-controlled dissolution, and
589 suggests the formation of Fe-organic complexes in solution under anoxic conditions (Figure 6).

590 The δ^{30}Si in soils (ranging from -1.32 to -0.38 ‰) decreases relative to the parent basalt (-0.29 ± 0.06
591 ‰, 2SD) with increasing degree of weathering and the formation of secondary aluminosilicates, and
592 more specifically with the evolution from poorly crystalline aluminosilicates such as allophane to

crystalline clay minerals such as kaolinite. Under oxic conditions and in fluctuating redox conditions, the heavier $\delta^{30}Si$ composition of soil solutions than soils ($\Delta^{30}Si_{solution-soil}$ = 0.92 ± 0.26 ‰) reflects the incorporation of light Si isotopes into secondary aluminosilicates. Under anoxic conditions, a larger $\Delta^{30}Si_{solution-soil}$ (1.63 ± 0.40 ‰) points to a succession of processes that preferentially incorporates light Si isotopes, i.e., the cumulative contribution of secondary clay minerals and amorphous silica precipitation. The precipitation of amorphous silica is confirmed and suggests that Si concentration in solution reached supersaturation with respect to amorphous silica due to Al affinity for organic ligands, thereby providing indirect support for the formation of metal-organic complexes in the poorly drained soils consistently with the conclusion based on Fe isotopes.

This study suggests that if the warming of peatlands at high latitude decreases soil drainage, Fe export from soils as Fe-organic complexes will increase. Further study is needed to quantify the implications of such enhanced Fe export from soils on the proportion of colloidal Fe in rivers and hence for Fe transport in rivers.

References

Abraham K., Opfergelt S., Fripiat F., Cavagna A.-J., de Jong J. T. M., Foley S., André L., Cardinal D. (2008) $\delta^{30}Si$ and $\delta^{29}Si$ determinations on USGS BHVO-1 and BHVO-2 reference materials via new configuration on Nu Plasma Multi Collector ICP-MS. *Geost. Geoanal. Res.* **32**, 193-202.

Akerman A., Poitrasson F., Oliva P., Audry S., Prunier J., Braun J.-J. (2014) The isotopic fingerprint of Fe cycling in an equatorial soil–plant–water system: The Nsimi watershed, South Cameroon. *Chem. Geol.* **385**, 104-116.

Arnalds O. (2004) Volcanic Soils of Iceland. *Catena* **56**, 3-20.

Arnalds O. (2008) Soils of Iceland. *Jokull* **58**, 409-421.

Arnalds O., Gíslason S. R. (2002) Validity of oxalate extraction for characterization and Al/Si calculations for vitric Andosols. Soil Resources of European Volcanic Systems. *Mainzer naturwiss. Archiv* **40**, 13-15.

Arnalds O., Gretarsson E. (2001) Soil Map of Iceland, Second Edition. Agricultural Research Institute, Reykjavik. Available in digital format, www.rala.is/desert.

Arnalds O., Gudmundsson J., Oskarsson H., Brink S.H., Gisladottir F.O. (2016) Icelandic inland wetlands: Characteristics and Extent of Draining. *Wetlands*, DOI 10.1007/s13157-016-0784-1.

636 Bascomb D.L. (1968) Distribution of pyrophosphate extractable iron and organic carbon in soils in various
637   groups. *J.Soil.Sci.* **19**, 251-268.
638 Beard B.L., Johnson C.M., Skulan J.L., Nealson K.H., Cox L., Sun H. (2003) Application of Fe isotopes to tracing
639   the geochemical and biological cycling of Fe. *Chem. Geol.* **195**, 87-117.
640 Bergquist B.A., Boyle E.A. (2006) Iron isotopes in the Amazon River system: Weathering and transport
641   signatures. *Earth Planet. Sci. Lett.* **248**, 54-68.
642 Blakemore L. C., Searle P. L., Daly B. K. (1981) Methods for Chemical Analysis of Soil. New Zealand Soil Bureau
643   Scientific Report 10 A, second revision.
644 Bonneville S., Van Cappellen P., Behrends T. (2004) Microbial reduction of iron(III) oxyhydroxides: effects of
645   mineral solubility and availability. *Chem. Geol.* **212**, 255-268.
646 Borggaard O.K. (1988) Phase Identification by Selective Dissolution Techniques. Iron in soils and clay minerals
647   (eds Stucki, J.W., Goodman, B.A., Schwertmann, U.), Nato Science Series C 217, 83-98.
648 Boyd P.W., Watson A.J., Law C.S., Abraham E.R., Trull T., Murdoch R. et al. (2000) A mesoscale phytoplankton
649   bloom in the polar Southern Ocean stimulated by iron fertilization. *Nature* **407**, 695-702.
650 Boyle E.A., Edmond J.M. (1977) The mechanism of iron removal in estuaries. *Geochim. Cosmochim. Acta* **41**,
651   1313-1324.
652 Brantley S.L., Liermann L., Bullen T.D. (2001) Fractionation of Fe isotopes by soil microbes and organic acids.
653   *Geology* **29**, 535-538.
654 Brantley S.L., Liermann L.J., Guynn R.L., Anbar A., Icopini G.A., Barling J. (2004) Fe isotopic fractionation during
655   mineral dissolution with and without bacteria. *Geochim. Cosmochim. Acta* **68**, 3189-3204.
656 Buettner S.W., Kramer M.G., Chadwick O.A., Thompson A. (2014) Mobilization of colloidal carbon during iron
657   reduction in basaltic soils. *Geoderma* **221–222**, 139-145.
658 Buss H.L., Mathur R., White A.F., Brantley S.L. (2010) Phosphorus and iron cycling in deep saprolite, Luquillo
659   Mountains, Puerto Rico. *Chem. Geol.* **269**, 52-61.
660 Caldelas C., Weiss D.J. (2017) Zinc Homeostasis and isotopic fractionation in plants: a review. *Plant Soil* **411**, 17–
661   46.
662 Chapman J.B., Weiss D.J., Shan Y., Lemburger M.(2009) Iron isotope fractionation during leaching of granite and
663   basalt by hydrochloric and oxalic acids. *Geochim. Cosmochim. Acta* **73**, 1312-1324.
664 Chauvel A., Lucas Y., Boulet R. (1987) On the genesis of the soil mantle of the region of Manaus, Central
665   Amazonia, Brazil. *Experientia* **43**, 234-241.
666 Chorover J., Kretzschmar R., Garcia-Pichel F., Sparks D. L. (2007) Soil biogeochemical processes within the
667   Critical Zone. *Elements* **3**, 321-326.
668 Cornelis J.-T., Delvaux B., Cardinal D., André L., Ranger J., Opfergelt S., 2010. Tracing mechanisms controlling
669   the release of dissolved silicon in forest soil solutions using Si isotopes and Ge/Si ratios. *Geochim.*
670   *Cosmochim. Acta* **74**, 3913-3924.
671 Cornelis J.T., Weis D., Lavkulich L., Vermeire M.-L., Delvaux B., Barling J. (2014) Silicon isotopes record
672   dissolution and re-precipitation of pedogenic clay minerals in a podzolic soil chronosequence.
673   *Geoderma* **235–236**, 19-29.
674 Cornell R.M., Schwertmann U. (2003) The iron oxides: Structure, properties, reactions, occurrence and uses.
675   2nd ed. VCH, Weinheim, Germany.
676 Cornu S., Besnault A., Bermond A. (2008) Soil podzolisation induced by reforestation as shown by sequential
677   and kinetic extractions of Fe and Al. *Eur. J.Soil Sci.* **59**, 222-232.
678 Cornu S., Clozel B. (2000) Extractions séquentielles et spéciation des éléments trace métalliques dans les sols
679   naturels : analyse critique. *Etudes et Gestion des Sols* **7**, 179-189.
680 Crochet P., Jóhannesson T., Jónsson T., Sigurðsson O., Björnsson H., Pálsson F., Barstad I. (2007) Estimating the
681   spatial distribution of precipitation in Iceland using a linear model of orographic precipitation. *J. of*
682   *Hydrometeorol.* **8**, 1285-1306.
683 Dauphas N., John G.J., Rouxel O. (2017) Iron isotope systematics. *Reviews in Mineralogy & Geochemistry* **82**,
684   415-510.
685 Delmelle P., Opfergelt S., Cornelis J-T., Ping C.L. (2015) Volcanic soils. In: *The Encyclopedia of Volcanoes*, Eds:
686   Sigurdsson H., Houghton B., Rymer H., Stix J., McNutt S., 2nd Edition, Academic Press, San Diego, 1253-
687   1264.

688 Delstanche S., Opfergelt S., Cardinal D., Elsass F., André L., Delvaux B. (2009) Silicon isotopic fractionation
689   during adsorption of aqueous monosilicic acid onto iron oxide. *Geochim. Cosmochim. Acta* **73**, 923-
690   934.
691 Dideriksen K., Baker J.A., Stipp S.L.S. (2008) Equilibrium Fe isotope fractionation between inorganic aqueous
692   Fe(III) and the siderophore complex, Fe(III)-desferrioxamine B. *Earth Planet. Sci. Lett.* **269**, 280-290.
693 Dietzel M. (2005) Impact of cyclic freezing on precipitation of silica in Me–SiO 2–H 2O systems and geochemical
694   implications for cryosoils. *Chem. Geol.* **216**, 79-88.
695 dos Santos Pinheiro G. M., Poitrasson F., Sondag F., Cochonneau G., Vieira L. C. (2014) Contrasting iron isotopic
696   compositions in river suspended particulate matter: the Negro and the Amazon annual river cycles.
697   *Earth Planet. Sci. Lett.* **394**, 168-178.
698 Emmanuel S., Erel Y., Matthews A., Teutsch N. (2005) A preliminary mixing model for Fe isotopes in soils. *Chem.*
699   *Geol.* **222**, 23-34.
700 Escoube R., Rouxel O.J., Pokrovsky O.S., Schroth A., Holmes R.M., Donard O.F.X. (2015) Iron isotope systematics
701   in Arctic rivers. *C. R. Geoscience* **347**, 377-385.
702 Fantle M.S., DePaolo, D.J. (2004) Iron isotopic fractionation during continental weathering. *Earth Planet. Sci.*
703   *Lett.* **228**, 547-562.
704 Fekiacova Z., Pichat S., Cornu S., Balesdent J. (2013) Inferences from the vertical distribution of Fe isotopic
705   compositions on pedogenetic processes in soils. *Geoderma* **209–210**, 110–118.
706 Fekiacova Z., Vermeire M.L., Bechon L., Cornelis J.T., Cornu S. (2017) Can Fe isotope fractionations trace the
707   pedogeneticmechanisms involved in podzolization? *Geoderma* **296**, 38-46.
708 Frings P.J., Clymans W., Fontorbe G., De La Rocha C.L., Conley D.J. (2016) The continental Si cycle and its impact
709   on the ocean Si isotope budget. *Chem. Geol*. **425**, 12-36.
710 Fritsch E., Allard T., Benedetti M.F., Bardy M., Do Nascimento N.R., Li Y., Calas G. (2009) Organic complexation
711   and translocation of ferric iron in podzols of the Negro River watershed. Separation of secondary Fe
712   species from Al species. *Geochim. Cosmochim. Acta* **73**, 1813-1825.
713 Fritsch E., Balan E., Do Nascimento N.R., Allard T., Bardy M., Bueno G., Derenne S., Melfi A.J., Calas G. (2011)
714   Deciphering the weathering processes using environmental mineralogy and geochemistry: Towards an
715   integrated model of laterite and podzol genesis in the Upper Amazon Basin. *C. R. Geoscience* **343**, 188-
716   198.
717 Garnier J., Garnier J.-M., Vieira C.L., Akerman A., Chmeleff J. Ruiz R.I., Poitrasson F. (2017) Iron isotope
718   fingerprints of redox and biogeochemical cycling in the soil-water-rice plant system of a paddy field.
719   *Sci. Tot. Environ.* **574**, 1622-1632.
720 Geilert S., Vroon P.Z., Keller N.S., Gudbrandsson S., Stefánsson A., van Bergen M.J. (2015) Silicon isotope
721   fractionation during silica precipitation from hot-spring waters: evidence from the Geysir geothermal
722   field, Iceland. *Geochim. Cosmochim. Acta* **164**, 403-427.
723 Geilert S., Vroon P.Z., Roerdink D.L., Cappellen P.V., van Bergen, M.J. (2014) Silicon isotope fractionation during
724   abiotic silica precipitation at low temperatures: inferences from flow-through experiments. *Geochim.*
725   *Cosmochim. Acta* **142**, 95-114.
726 Georg R.B., Reynolds B.C., Frank M., Halliday A.N. (2006) New sample preparation techniques for the
727   determination of Si isotopic compositions using MC-ICPMS. *Chem. Geol.* **235**, 95-104.
728 Georg R.B., Zhu C., Reynolds B.C., Halliday A.N. (2009) Stable silicon isotopes of groundwater, feldspars, and
729   clay coatings in the Navajo Sandstone aquifer, Black Mesa, Arizona, USA. *Geochim. Cosmochim. Acta*
730   **73**, 2229-2241.
731 Guelke M., von Blanckenburg F. (2007) Fractionation of stable iron isotopes in higher plants. *Environ. Sci.*
732   *Technol.* **41**, 1896-1901.
733 Guelke M., von Blanckenburg F., Schoenberg R., Staubwasser M., Stuetzel H. (2010) Determining the stable Fe
734   isotope signature of plant-available iron in soils. *Chem. Geol.* **277**, 269-280.
735 Guelke-Stelling M., von Blanckenburg F. (2012) Fe isotope fractionation caused by translocation of iron during
736   growth of bean and oat as models of strategy I and II plants. *Plant Soil* **352**, 217-23.
737 Guicharnaud R. A. (2009) Biogeochemistry of Icelandic Andosols. Ph. D. thesis, University of Aberdeen,
738   Aberdeen, UK. p. 140.
739 Hecht B.P., Vogt K.A., Eysteinsson P., Vogt D.J. (2007) Changes in air and soil temperatures in three Icelandic
740   birch forests with different land-use histories. *Icel. Agric.Sci.* **20**, 49-60.

741 Henkel S., Kasten S., Poulton S. W., Staubwasser M. (2016) Determination of the stable iron isotopic
742   composition of sequentially leached iron phases in marine sediments. *Chem. Geol.* **421**, 93-102.
743 Herbillon A. J. (1986) Chemical estimation of weatherable minerals present in the diagnostic horizons of low
744   activity clay soils. In: *Proceedings of the 8th International Soil Classification Workshop: Classification,*
745   *Characterization and Utilization of Oxisols*, Part 1 (eds. F. H. Beinroth, M. N. Camargo and Eswaran).
746   EMBRAPA, Rio de Janeiro, pp. 39-48.
747 Hiemstra T., Barnett M. O., van Riemsdijk W. H. (2007) Interaction of silicic acid with goethite. *J. Colloid*
748   *Interface Sci.* **310**, 8-17.
749 Ilina S.M., Poitrasson F., Lapitskiy S.A., Alekhin Y.V., Viers J., Pokrovsky O.S. (2013) Extreme iron isotope
750   fractionation between colloids and particles of boreal and temperate organic-rich waters. *Geochim.*
751   *Cosmochim. Acta* **101**, 96-111.
752 Ingri J., Malinovskiy D., Rodushkin I., Baxter D., Widerlund A., Andersson P., Gustafsson O., Forsling W. (2006)
753   Iron isotope fractionation in river colloidal matter. *Earth Planet. Sci. Lett.* **245**, 792-798.
754 IPCC (2013) Climate Change 2013: The Physical Science Basis. Contribution of Working Group I to the Fifth
755   Assessment Report of the Intergovernmental Panel on Climate Change (eds. Stocker, T.F. et al)
756   Cambridge University Press, 1535 pp.
757 IUSS Working Group WRB (2014) World Reference Base for Soil Resources 2014. International soil classification
758   system for naming soils and creating legends for soil maps. FAO, Rome.
759 Jeanroy E., Guillet B. (1981) The occurence of suspended ferruginous particles in pyrophosphate extracts of
760   some soil horizons. *Geodema* **26**, 95-105.
761 Johannesson T., Eiriksson T., Gudmundsdottir K.B., Sigurdarson S., Kristinsson J. (2007) Overview: Seven trace
762   elements in Icelandic forage. Their value in animal health and with special relation to scrapie. *Icel.*
763   *Agric. Sci.* **20**, 3-24.
764 Johnson C.M., Skulan J.L., Beard B.L. et al. (2002) Isotopic fractionation between Fe(III) and Fe(II) in aqueous
765   solutions. *Earth Planet. Sci. Lett.* **195**, 141-153.
766 Johnson C.M., Beard B.L., Roden E.E. (2008) The Iron Isotope Fingerprints of Redox and Biogeochemical Cycling
767   in Modern and Ancient Earth. *Annu. Rev. Earth Planet. Sci.* **36**, 457-493.
768 Jones L. H. P., Handreck K. A. (1963) Effects of iron and aluminium oxides on silica in solution in soils. *Nature*
769   **198**, 852-853.
770 Kiczka M., Wiederhold J.G., Frommer J., Kraemer S.M., Bourdon B., Kretzschmar R. (2010a) Iron isotope
771   fractionation during proton- and ligand-promoted dissolution of primary phyllosilicates. *Geochim.*
772   *Cosmochim. Acta* **74**, 3112-3128.
773 Kiczka M., Wiederhold J.G., Frommer J., Kraemer S.M., Bourdon B., Kretzschmar R. (2010b) Iron isotope
774   fractionation during Fe uptake and translocation in alpine plants. *Environ. Sci. Technol.* **44**, 6144-6150.
775 Kiczka M., Wiederhold J.G., Frommer J., Voegelin A., Kraemer S.M., Bourdon B., Kretzschmar R. (2011) Iron
776   speciation and isotope fractionation during silicate weathering and soil formation in an alpine glacier
777   forefield chronosequence. *Geochim. Cosmochim. Acta* **75**, 5559-5573.
778 Kostka J. E., Luther G.W. (1994) Partitioning and speciation of solid phase iron in saltmarsh sediments.
779   *Geochim. Cosmochim. Acta* **58**, 1701-1710.
780 Krachler R., Jirsa F., Ayromlou S. (2005) Factors influencing the dissolved iron input by river water to the open
781   ocean. *Biogeosciences* **2**, 311-315.
782 Krachler R., Krachler R.F., von der Kammer F., Süphandag A., Jirsa F., Ayromlou S., Hofmann T., Keppler B.K.
783   (2010) Relevance of peat-draining rivers for the riverine input of dissolved iron into the ocean. Sci. Tot.
784   Envi. **408**, 2402-2408.
785 Li Y., Ding T.P., Wan D. (1995) Experimental study of silicon isotope dynamic fractionation and its application
786   in geology. *Chin. J. Geochem.* **14**, 212-219.
787 Liu S.A., Teng F.Z., Li S., Wei G.J., Ma J.L., Li D. (2014) Copper and iron isotope fractionation during weathering
788   and pedogenesis: Insights from saprolite profiles. *Geochim. Cosmochim. Acta*, **146**, 59-75.
789 Lucas Y., Boulet R., Chauvel A., Veillon L. (1987) Systèmes sols ferrallitiques - Podzols en région amazonienne.
790   In: Righi D., Chauvel A. (Eds.), *Podzols et Podzolisation.* AFES et INRA, Plaisir et Paris, 53-65.
791 Mansfeldt T., Schuth S., Häusler W., Wagner F., Kaufhold S., Overesch M. (2012) Iron oxide mineralogy and
792   stable iron isotope composition in a Gleysol with petrogleyic properties. *J. Soil Sedim.: Protection, Risk*
793   *Assessment, & Remediation* **12**, 97-114.
794 Marschner H., Römheld, V. (1994) Strategies of plants for acquisition of iron. *Plant Soil* **165**, 261-274.

795   Martin J. H., Fitzwater S. E. (1988) Iron-deficiency limits phytoplankton growth in the Northeast Pacific
796   Subarctic. *Nature* **331**, 341-342.
797   McKeague J. A., Cline M. G. (1963) Silica in soils. *Adv. Agron*. **15**, 339-396.
798   Mehra O. P., Jackson M. L. (1960) Iron oxides removal from soils and clays by dithionite-citrate system buffered
799   with sodium bicarbonate. *Proc. 7th Natl. Conf. Clays Clay Minerals*, Washington. pp. 317-327.
800   Melton E. D., Swanner E. D., Behrens S., Schmidt C., Kappler A. (2014) The interplay of microbially mediated
801   and abiotic reactions in the biogeochemical Fe cycle. *Nature Reviews Microbiology* **12**, 797-808.
802   Millet M.-A., Baker J.A., Payne C.E. (2012) Ultra-precise stable Fe isotope measurements by high resolution
803   multiple-collector inductively coupled plasma mass spectrometry with a 57Fe–58Fe double spike.
804   *Chem. Geol.* **304**, 18-25.
805   Mizota C., van Reeuwijk L.P. (1989) Clay Mineralogy and Chemistry of Soils Formed in Volcanic Material in
806   Diverse Climatic Regions. Soil Monograph 2. ISRIC, Wageningen.
807   Morel F.M.M., Rueter J.G., Price N.M. (1991) Iron nutrition of phytoplankton and its possible importance in the
808   ecology of ocean regions with high nutrient and low biomass. *Oceanography* **4**, 56-61.
809   Morgan J.L., Wasylenki L.E., Nuester J., Anbar A.D. (2010) Fe Isotope Fractionation during Equilibration of Fe-
810   Organic Complexes. *Environ. Sci. Technol.* **44**, 6095-6101.
811   Mulholland D. S., Poitrasson F., Boaventura G. R., Allard T., Vieira L. C., Santos R. V., Mancini L., Seyler P. (2015)
812   Insights into iron sources and pathways in the Amazon River provided by isotopic and spectroscopic
813   studies. *Geochim. Cosmochim. Acta* **150**, 142-159.
814   Oelkers E.H., Gislason S.R. (2001) The mechanism, rates and consequences of basaltic glass dissolution. I: An
815   experimental study of the dissolution rates of basaltic glass as a function of aqueous Al, Si and oxalic
816   acid concentration at 25°C and pH = 3 and 11. *Geochim. Cosmochim. Acta* **65**, 3671-3681.
817   Oelze M., von Blanckenburg F., Bouchez J., Hoellen D., Dietzel M. (2015) The effect of Al on Si isotope
818   fractionation investigated by silica precipitation experiments. *Chem. Geol.* **397**, 94-105.
819   Oelze M., von Blanckenburg F., Hoellen D., Dietzel M., Bouchez J. (2014) Si stable isotope fractionation during
820   adsorption and the competition between kinetic and equilibrium isotope fractionation: implications
821   for weathering systems. *Chem. Geol.* **380**, 161-171.
822   Opfergelt S., Burton K.W., Georg R.B., West A.J., Guicharnaud R., Sigfusson B., Siebert C., Gislason S.R., Halliday
823   A.N. (2014) Magnesium retention on the soil exchange complex controlling Mg isotope variations in
824   soils, soil solutions and vegetation in volcanic soils, Iceland. *Geochim. Cosmochim. Acta* **125**, 110-130.
825   Opfergelt S., Cardinal D., André L., Delvigne C., Bremond L., Delvaux B. (2010) Variations of δ^{30}Si and Ge/Si with
826   weathering and biogenic input in tropical basaltic ash soils under monoculture. *Geochim. Cosmochim.*
827   *Acta* **74**, 225-240.
828   Opfergelt S., de Bournonville G., Cardinal D., André L., Delstanche S., Delvaux B. (2009) Impact of soil
829   weathering degree on silicon isotopic fractionation during adsorption onto iron oxides in basaltic ash
830   soils, Cameroon. *Geochim. Cosmochim. Acta* **73**, 7226-7240.
831   Opfergelt S., Delmelle P. (2012) Silicon isotopes and continental weathering processes: assessing controls on Si
832   transfer to the ocean. *CR Geoscience* **344**, 723-738.
833   Opfergelt S., Georg R.B., Burton K.W., Guicharnaud R., Siebert C., Gislason S.R., Halliday A.N. (2011) Silicon
834   isotopes in allophane as a proxy for mineral formation in volcanic soils. *Applied Geochem.* **26**, S115-
835   S118.
836   Opfergelt S., Georg R.B., Delvaux B., Cabidoche Y.M., Burton K.W., Halliday A.N. (2012) Silicon isotopes and the
837   tracing of desilication in volcanic soil weathering sequences, Guadeloupe. *Chem. Geol.* **326-327**, 113-
838   122.
839   Opfergelt S., Cornelis J.T., Houben D., Givron C., Burton K.W., Mattielli N. (2017) The influence of weathering
840   and soil organic matter on Zn isotopes in soils. *Chem. Geol.* **466**, 140-148.
841   Orradottir B., Archer S. R., Arnalds O., Wilding L. P., Thurow T. L. (2008) Infiltration in Icelandic Andisols: the
842   role of vegetation and soil frost. *Arc. Antarc. Alp. Res.* **40**, 412-421.
843   Paque M., Detienne M., Maters E C.., Delmelle P. (2016) Smectites and zeolites in ash from the 2010 summit
844   eruption of Eyjafjallajökull volcano, Iceland. *Bull Volcanol*. **78**, 61.
845   Parfitt R.L. (2009) Allophane and imogolite : role in soil biogeochemical processes. *Clay Miner.* **44**, 135-155.
846   Parfitt R.L., Childs C.W. (1988) Estimation of forms of Fe and Al - a review, and analysis of contrasting soils by
847   dissolution and Mossbauer methods. *Aust. J. Soil Res.* **26**, 121-144.
848   Parfitt R.L., Kimble J.M. (1989) Conditions for formation of allophane in soils. *Soil Sci. Soc. Am. J.* **53**, 971-977.

849   Pearce C.R., Burton K.W., Pogge von Strandmann P.A.E., James R.H., Gislason S.R. (2010) Molybdenum isotope
850   behaviour accompanying continental weathering and riverine transport in a basaltic terrain. *Earth
851   Planet. Sci. Lett.* **295**, 104-114.
852   Ping C.L., Shoji S., Ito T. (1988) Properties and classification of three volcanic ash derived pedons from Aleutian
853   Islands and Alaska Peninsula, Alaska. *Soil Sci. Soc. Am. J.* **52**, 455-462.
854   Pogge Von Strandmann P. A. E., Burton K. W., James R. H., Van Calsteren P., Gislason S. R., Sigfusson B. (2008)
855   The influence of weathering processes on riverine magnesium isotopes in a basaltic terrain. *Earth
856   Planet. Sci. Lett.* **276**, 187-197.
857   Pogge von Strandmann P.A.E., Burton K.W., James R.H., van Calsteren P., Gislason S.R., Mokadem F. (2006)
858   Riverine behaviour of uranium and lithium isotopes in an actively glaciated basaltic terrain. *Earth
859   Planet. Sci. Lett.* **251**, 134-147.
860   Poitrasson F. (2017) Silicon isotope geochemistry. *Reviews in Mineralogy & Geochemistry* **82**, 289-344.
861   Poitrasson F., Viers J., Martin F., Braun J.-J. (2008) Limited iron isotope variations in recent lateritic soils from
862   Nsimi, Cameroon: implications for the global Fe geochemical cycle. *Chem. Geol.* **253**, 54-63.
863   Poulton S.W., Raiswell R. (2002) The low-temperature geochemical cycle of iron: from continental fluxes to
864   marine sediment deposition. *Am. J. Sci.* **302**, 774-805.
865   Rai D., Kittrick J.A. (1989) Mineral equilibria and the soil system. Minerals in Soil Environments (eds J. Dixon & S.
866   Weed), pp. 161-198. Soil Science Society of America, Madison, WI, USA.
867   Reynolds B.C., Aggarwal J., André L., Baxter D., Beucher C., Brzezinski M.A., Engström E., Georg R.B., Land M.,
868   Leng M.J., Opfergelt S., Rodushkin I., Sloane H.S., van den Boorn S.H.J.M., Vroon P.Z., Cardinal D.
869   (2007) An inter-laboratory comparison of Si isotope reference materials. J. Anal. Atom. Spectrom. **22**,
870   561-568.
871   Roerdink D.L., van den Boorn S.H., Geilert S., Vroon P.Z., van Bergen M.J. (2015) Experimental constraints on
872   kinetic and equilibriumsilicon isotope fractionation during the formation of non-biogenic chert
873   deposits. *Chem. Geol.* **402**, 40-51.
874   Romanovsky V. E., Smith S. L., Christiansen H. H. (2010) Permafrost thermal state in the polar Northern
875   Hemisphere during the International Polar Year 2007-2009: a synthesis. *Permafrost Periglac. Process.*
876   **21**, 106-116.
877   Rouiller J., Burtin G., Souchier B. (1972) La dispersion des sols dans l'analyse granulométrique. Méthode
878   utilisant les résines échangeuses d'ions. ENSAIA Nancy 14, 194-205.
879   Ryan J.N., Gschwend P.M. (1991) Extraction of Iron Oxides from Sediments Using Reductive Dissolution by
880   Titanium(III). *Clays Clay Min.* **39**, 509-518.
881   Savage P.S., Georg R.B., Armytage R.M.G., Williams H.M., Halliday A.N. (2010) Silicon isotope homogeneity in
882   the mantle. *Earth Planet. Sci. Lett.* **295**, 139-146.
883   Schauble E. (2004) Applying stable isotope fractionation theory to new systems. *Rev. Mineral. Geochem.* **55**, 65-
884   111.
885   Schulz M., Stonestrom D., Lawrence C., Bullen T., Fitzpatrick J., Kyker-Snowman E., Manning J., Mnich M. (2016)
886   Structured heterogeneity in a marine terrace chronosequence: Upland mottling. *Vadose Zone J.* **15** (2),
887   doi:10.2136/vzj2015.07.0102.
888   Schuth S., Hurrass J., Munker C., Mansfeldt T. (2015) Redox-dependent fractionation of iron isotopes in
889   suspensions of a groundwater-influenced soil. *Chem. Geol.* **392**, 74-86.
890   Schuth S., Mansfeldt T. (2015) Iron isotope composition of aqueous phases of a lowland environment. *Environ.
891   Chem.* **13**, 89-101.
892   Schwertmann U. (2008) Iron oxides. Encyclopedia of Soil Science (ed. W. Chesworth), pp. 363-369. Springer,
893   Dordrecht, the Netherlands.
894   Shoji S., Masui J.-I. (1971) Opaline silica of recent volcanic ash soils in Japan. *J. Soil Sci.* **22**, 101-108.
895   Siebert C., Pett-Ridge J., Opfergelt S., Guicharnaud R., Halliday A.N., Burton K.W. (2015) Molybdenum isotope
896   fractionation in soils: influence of redox conditions, organic matter, and atmospheric inputs. *Geochim.
897   Cosmochim. Acta* **162**, 1-24.
898   Sigfusson B., Gislason S. R., Paton G. I. (2008) Pedogenesis and weathering rates of a Histic Andosol in Iceland:
899   field and experimental soil solution study. *Geoderma* **144**, 572-592.
900   Smetacek V., Klaas C., Strass V.H., Assmy P., Montresor M., Cisewski B. et al. (2012) Deep carbon export from a
901   Southern Ocean iron-fertilized diatom bloom. *Nature* **487**, 313-319.

902 Steinhoefel G., Breuer J., von Blanckenburg F., Horn I., Michael Sommer M. (2017) The dynamics of Si cycling
903   during weathering in two small catchments in the Black Forest (Germany) traced by Si isotopes. *Chem.*
904   *Geol.* **466**, 389-402.
905 Swedlund P. J., Webster J. G. (1999) Adsorption and polymerisation of silicic acid on ferrihydrite, and its effect
906   on arsenic adsorption. *Water Res.* 33, 3413-3422.
907 Swindles G.T., Morris P.J., Mullan D., Watson E.J., Turner T.E. et al., (2015) The long-term fate of permafrost
908   peatlands under rapid climate warming. *Scientific Reports* **5**, 17951.
909 Thompson A., Ruiz J., Chadwick O.A., Titus M., Chorover J. (2007) Rayleigh fractionation of iron isotopes during
910   pedogenesis along a climate sequence of Hawaiian basalt. *Chem. Geol.* **238**, 72-83.
911 Thompson A., Rancourt D.G., Chadwick O.A., Chorover J. (2011) Iron solid-phase differentiation along a redox
912   gradient in basaltic soils. *Geochim. Cosmochim. Acta* **75**, 119-133.
913 Walker A.L. (1983) The Effects of Magnetite on Oxalate- and Dithionite-Extractable Iron, *Soil Sci. Soc. Am. J.* **47**,
914   1022-1026.
915 Welch S.A., Beard B.L., Johnson C.M., Braterman P.S. (2003) Kinetic and equilibrium Fe isotope fractionation
916   between aqueous Fe(II) and Fe(III). *Geochim. Cosmochim. Acta* **67**, 4231-4250.
917 Westermann S., Østby T., Gisnås K., Schuler T. V., Etzelmüller B. (2015) A ground temperature map of the North
918   Atlantic permafrost region based on remote sensing and reanalysis data. *The Cryosphere Disc.* **9**, 753-
919   790.
920 Weyer S., Anbar A.D., Brey G.P., Munker C., Mezger K., Woodland A.B. (2005) Iron isotope fractionation during
921   planetary differentiation. *Earth Planet. Sci. Lett.* **240**, 251-264.
922 Wiederhold J.G., Teutsch N., Kraemer S.M., Halliday A.N., Kretzschmar R. (2007a) Iron isotope fractionation
923   during pedogenesis in redoximorphic soils. *Soil Sci. Soc. Am. J.* **71**, 1840-1850.
924 Wiederhold J.G., Teutsch N., Kraemer S.M., Halliday A.N., Kretzschmar R. (2007b) Iron isotope fractionation in
925   oxic soils by mineral weathering and podzolisation. *Geochim. Cosmochim. Acta* **71**, 5821-5833.
926 Wiederhold J.G., Kraemer S.M., Teutsch N., Borer P.M., Halliday A.N., Kretzschmar R. (2006) Iron Isotope
927   Fractionation during Proton-Promoted, Ligand-Controlled, and Reductive Dissolution of Goethite.
928   *Environ. Sci. Technol.* **40**, 3787-3793.
929 Williams H.M., Bizimis M. (2014) Iron isotope tracing of mantle heterogeneity within the source regions of
930   oceanic basalts. *Earth Planet. Sci. Lett.* **404**, 396-407.
931 Williams H.M., Wood B.J., Wade J., Frost D., Tuff J. (2012) Isotopic evidence for internal oxidation of the Earth's
932   mantle. *Earth Planet. Sci. Lett.*, 321-322, 54-63.
933 Wolff-Boenisch D., Gislason S.R., Oelkers E.H. (2004) The effect of fluoride on the dissolution rates of natural
934   glasses at pH 4 and 25°C. *Geochim. Cosmochim. Acta* **68**, 4571-4582.
935 Wu L., Beard B.L., Roden E.E., Johnson C.M. (2011) Stable iron isotope fractionation between aqueous Fe(II)
936   and hydrous ferric oxide. *Envi. Sci. Tech.* **45**, 1847-1852.
937 Yeghicheyan D., Carignan J., Valladon M., Bouhnik Le Coz M., Le Cornec F., Castrec-Rouelle M., Robert M.,
938   Aquilina L., Aubry E., Churlaud C., Dia A., Deberdt S., Dupré B., Freydier R., Gruau G., Hénin O., de
939   Kersabiec A.-M., Macé J., Marin L., Morin N., Petitjean P., Serrat E. (2001) A compilation of silicon and
940   thirty one trace elements measured in the natural river water reference material SLRS-4 (NRC-CNRC).
941   *Geostand. Geoanal. Res.* **25**, 465-474.
942 Yesavage T., Stinchcombb G.E., Fantle M.S., Sakd P.B., Kasznele A., Brantley S.L. (2016) Investigation of a
943   diabase-derived regolith profile from Pennsylvania: Mineralogy, chemistry and Fe isotope
944   fractionation. *Geoderma* **273**, 83-97.
945 Yesavage T.A., Fantle M.S., Vervoort J., Mathur R., Jin L., Liermann L.J., Brantley S.L. (2012) Fe cycling in the
946   Shale Hills Critical Zone Observatory, Pennsylvania: an analysis of biogeochemical weathering and Fe
947   isotope fractionation. *Geochim. Cosmochim. Acta* **99**, 18-38.
948 Zambardi T., Poitrasson F. (2011) Precise Determination of silicon isotopes in silicate rock reference materials
949   by MC-ICP- MS. *Geostand. Geoanal. Res.* **35**, 89-99.
950 Ziegler K., Chadwick O.A., Brzezinski M.A., Kelly E.F. (2005) Natural variations of δ^{30}Si ratios during progressive
951   basalt weathering, Hawaiian Islands. *Geochim. Cosmochim. Acta* **69**, 4597-4610.
952
953

Figure captions

Figure 1. Location map of the soil sites (HA, H, BA, GA, V) and the river sites (A3, A4, and HA) in Iceland studied here. Histic Andosol, HA; Histosol, H; Haplic Andosol, BA; Gleyic Andosol, GA; Vitric Andosol, V. Soil types are classified according to the World Reference Base for Soil Resources (IUSS, 2014). The soil map is based on Arnalds (2004) and Arnalds and Gretarsson (2001).

Figure 2. The degree of weathering in soils: The HA–H soils, with low Total Reserve in Bases (TRB = [Na] + [Mg] + [Ca] + [K]; Herbillon, 1986; data from Opfergelt et al., 2014) and a high proportion of free iron (Fe_d/Fe_t) are more weathered than V–BA–GA soils with higher TRB and lower Fe_d/Fe_t (Fe_d = Fe extracted by DCB or dithionite-citrate-bicarbonate; Fe_t = Fe total). Soil acronyms as in Figure 1.

Figure 3. (a) The relation between the Fe isotope composition in bulk soils ($\delta^{57}Fe_{bulk\ soil}$, 2SD) and the proportion of free iron (Fe_d/Fe_t, with Fe_d = Fe extracted by DCB or dithionite-citrate-bicarbonate; Fe_t = Fe total), the $\delta^{57}Fe$ of the basalt BIR-1 considered as representative of the parent material is given by the horizontal line for comparison; (b) The relation between the Fe isotope composition of the free iron pool extracted by DCB ($\delta^{57}Fe_{DCB}$, 2SD) and the $\delta^{57}Fe_{bulk\ soil}$, 2SD; a 1:1 line is provided for comparison; (c) The relation between the Fe isotope composition of the soil solution ($\delta^{57}Fe_{soil\ solution}$, 2SD) and the $\delta^{57}Fe_{bulk\ soil}$, 2SD; a 1:1 line is provided for comparison, and the two horizons with the highest Fe soil solution concentrations, H O4 and H O6, are identified (Table 2). Soil acronyms as for Figure 1 (no data available for V).

Figure 4. (a) The Si isotope composition in the bulk soils ($\delta^{30}Si_{bulk\ soil}$, 2SD) decreases with increasing degree of soil weathering, as shown by the proportion of free iron (Fe_d/Fe_t, with Fe_d = Fe extracted by DCB or dithionite-citrate-bicarbonate; Fe_t = Fe total), from V to BA-GA to HA-H. The $\delta^{30}Si$ of the parent basalt is given by the horizontal line for comparison. (b) The Si isotope composition of the clay fractions ($\delta^{30}Si_{clay}$, 2SD; < 2 μm) as a function of the $\delta^{30}Si_{bulk\ soil}$, 2SD; a 1:1 line is provided for comparison. (c) The Si isotope composition of the soil solution ($\delta^{30}Si_{soil\ solution}$, 2SD) as a function of the $\delta^{30}Si_{bulk\ soil}$, 2SD; a 1:1 line is provided for comparison, and the two horizons with the highest $\delta^{30}Si_{soil\ solution}$, H O4 and H O6, are identified (Table 2). Soil acronyms as for Fig. 1 (no data available for V in the clay fraction and in soil solution).

Figure 5. (a) Comparison between the main terrestrial Fe isotope variations ($\delta^{57}Fe$) in igneous rocks, soils and rivers in the literature and the present study. (b) Comparison between the main terrestrial Si isotope variations ($\delta^{30}Si$) in igneous rocks, soils, clay fractions, clay fractions from Cameroon with and without Fe-oxides, and soil solutions in the literature and the present study. [1] Beard et al., 2003, [2] Fantle & De Paolo 2004, [3] Emmanuel et al., 2005, [4] Fekiacova et al., 2013, [5] Mansfeldt et al., 2012, [6] Liu et al., 2014, [7] Fekiacova et al., 2017, [8] Thompson et al., 2007, [9] Akerman et al., 2014, [10] Schulz et al., 2016, [11] Wiederhold et al., 2007b, [12] Kiczka et al., 2011, [13] Yesavage et al., 2012, [14] Schuth and Mansfeldt 2015, [15] Garnier et al 2017, [16] Bergquist & Boyle 2006, [17] Mulholland et al., 2015, [18] Ilina et al., 2013, [19] Escoube et al., 2015, [20] Ingri et al., 2006, [21] review in Opfergelt and Delmelle, 2012, [22] review in Frings et al., 2016. Results expressed as $\delta^{56}Fe$ in the literature were converted to $\delta^{57}Fe$ using the mass-dependent scaling factor of 1.5.

Figure 6. Conceptual view (no scale) of the main processes controlling Fe release from soils based on the difference in Fe and Si isotope composition between soil solutions and bulk soils (e.g., $\Delta^{30}Si_{solution-}$

995   $_{soil} = \delta^{30}Si_{soil\ solution} - \delta^{30}Si_{bulk\ soil}$). Schematic soil constituents modified from Chorover et al., 2007. Soil
996   acronyms as for Figure 1.

Table 1

Table 1. Soil parameters (pH, carbon and clay content), bulk soil Fe and Si content (Fe$_t$, Si$_t$), Fe and Si content in selective extracts (dithionite-citrate-bicarbonate = d, oxalate = o, pyrophosphate = p) in soils. Iron and silicon isotope compositions of the bulk soils, secondary phases (Fe-oxides Fe$_d$ from DCB extracts for Fe isotopes, and clay fractions <2µm for Si isotopes), parent basalt, and grass from the site of HA profile. Soil acronyms as in Fig. 1.

Soil horizon		Depth	pH$_{H2O}$[a]	Carbon[a]	Clay[a]	Fe$_t$[a]	Si$_t$[a]	Fe$_d$	Fe$_o$	Fe$_p$	Si$_d$	Si$_o$	C$_p$	δ^{57}Fe$_{bulk\ soil}$	2SD[b]	δ^{57}Fe$_{DCB}$	2SD[b]	δ^{30}Si$_{bulk\ soil}$	2SD	δ^{30}Si$_{clay}$	2SD
		cm		%	%	g kg^{-1}	g kg^{-1}	g kg^{-1}	g kg^{-1}	g kg^{-1}	g kg^{-1}	g kg^{-1}	g kg^{-1}	‰	‰	‰	‰	‰	‰	‰	‰
HA	A1	0-15	5.32	18.52	56.1	165.7	83.4	129.2	41.5	43.5	3.7	8.2	56.6	0.38	0.08	-	-	-1.05	0.09	-1.73	0.10
HA	A2	15-26	4.89	16.94	54.3	98.9	110.7	71.5	31.6	27.0	4.0	15.9	52.3	0.12	0.03	0.25	*0.07*	-0.97	0.04	-1.64	0.17
HA	Bw1	26-40	4.82	14.49	55.2	175.1	98.0	139.2	70.0	33.1	5.5	13.9	45.0	-0.33	*0.07*	-0.51	*0.07*	-1.32	0.05	-1.84	0.15
HA	Bw2	40-57	5.15	16.86	45.5	164.4	97.2	129.8	41.6	32.6	4.7	11.5	47.1	-0.36	0.14	-0.43	*0.07*	-1.00	0.07	-2.04	0.14
HA	O1	57-67	4.44	28.71	53.8	55.7	55.6	50.9	25.6	18.7	4.5	11.0	74.0	-0.16	0.15	-0.19	*0.07*	-0.77	0.12	-1.11	0.14
HA	redox	67-83	4.27	12.79	-	57.6	185.4	14.0	8.3	3.7	2.2	11.5	30.2	-0.05	0.05	-0.71	*0.07*	-0.42	0.14	-	-
HA	O2	83+	3.93	42.73	55.3	42.9	32.0	40.9	19.1	16.0	1.9	2.4	82.5	-0.60	0.07	-0.79	*0.07*	-0.85	0.04	-	-
H	O1	0-13	6.18	21.00	52.3	120.3	100.4	99.5	39.8	11.5	3.7	4.1	29.6	0.67	*0.07*	-0.11	0.04	-0.82	0.09	-	-
H	O2	13-26	5.10	22.94	8.4	83.8	94.9	57.9	22.6	18.2	2.4	3.0	30.3	0.56	*0.07*	0.71	0.02	-1.08	0.05	-	-
H	O3	26-40	4.57	18.62	38.2	141.7	91.5	111.4	34.6	53.1	4.5	11.1	49.5	-0.02	0.02	-0.05	*0.07*	-0.73	0.15	-1.42	0.15
H	O4	52-63	4.66	10.32	44.4	101.6	157.6	79.1	19.6	35.5	3.4	7.6	30.6	0.12	*0.07*	0.16	0.05	-0.47	0.08	-0.97	0.15
H	O5	63-72	4.35	29.27	70.9	140.7	40.9	-	27.8	69.1	4.4	3.8	59.7	0.30	0.06	-	-	-0.68	0.06	-	-
H	O6	72+	4.56	30.39	42.7	86.6	48.8	-	23.0	41.8	3.5	5.9	57.8	0.44	0.01	-	-	-0.69	0.09	-	-
BA	A1	0-21	6.35	7.29	33.2	111.9	158.1	53.4	45.9	6.8	2.6	17.9	22.4	0.08	0.08	0.08	*0.07*	-0.53	0.03	-1.07	0.18
BA	A2	21-40	6.40	7.92	29.7	117.2	151.8	62.9	50.5	8.3	2.9	18.3	21.3	0.12	0.10	0.00	*0.07*	-0.72	0.07	-	-
BA	Bw1	40-52	6.50	6.47	37.2	122.7	150.2	58.3	43.1	6.3	3.2	15.4	16.6	0.14	0.04	-	-	-0.67	0.08	-	-
BA	Bw2	52-96	6.53	7.25	41.0	126.1	151.8	74.9	57.3	7.1	4.2	21.7	19.1	0.17	0.10	0.19	*0.07*	-0.61	0.06	-1.22	0.16
BA	Bw3/C	96+	6.24	5.71	-	127.9	153.4	59.4	49.7	6.9	3.3	21.0	20.7	0.12	0.06	-0.01	*0.07*	-0.57	0.10	-	-
GA	A1	0-12	6.22	9.51	37.1	104.5	135.4	52.8	43.4	6.8	3.7	16.3	25.4	0.10	0.04	0.05	0.07	-0.63	0.06	-1.11	0.14
GA	A2	12-29	6.30	6.20	41.2	119.2	149.9	64.4	50.0	5.1	4.4	20.4	16.7	0.10	*0.07*	-	-	-0.61	0.05	-	-
GA	Bw1	29-43	6.33	6.86	38.9	116.7	145.7	59.6	37.7	3.8	3.1	24.4	15.8	0.14	0.05	-0.03	0.07	-0.69	0.09	-0.85	0.13
GA	Bw2	43-56	6.34	6.76	36.3	105.5	155.5	49.6	27.3	2.4	3.0	25.7	14.9	-	-	-1.07	0.04	-0.58	0.06	-	-
GA	C	56-64	6.57	2.70	-	119.2	189.0	30.6	23.4	1.6	2.6	12.3	5.2	-0.09	0.05	-	-	-0.55	0.08	-	-
GA	2Bw1	64+	6.44	3.26	22.9	59.2	176.6	11.4	10.7	0.6	3.6	35.2	7.5	0.01	0.05	-0.23	0.02	-0.59	0.02	-0.63	0.09
V	A	0-9	7.77	0.32	4.6	116.2	203.2	18.3	22.7	0.6	2.9	14.8	2.1	-	-	-	-	-0.40	0.06	-	-
V	B/C	9-33	8.20	0.26	4.6	122.2	196.8	32.2	41.9	0.3	4.0	23.7	0.9	-	-	-	-	-0.47	0.08	-	-
V	C	33+	7.70	-	-	-	-	-	-	-	-	-	-	-	-	-	-	-0.38	0.09	-	-
Parent basalt			-	-	-	103.8	228.4	-	-	-	-	-	-	-	-	-	-	-0.29	0.06	-	-
Icelandic grass			-	-	-	-	-	-	-	-	-	-	-	-0.09	0.03	-	-	-	-	-	-

[a] data from Opfergelt et al., 2014; [b] in *italic* : for analyses where there was only enough Fe for 1 replicate, the 2SD of the in-house FeCl salt standard measured during the course of analysis is used

Table 2

Table 2. Characterization of the soil solutions: pH in solution, iron and silicon concentrations in solution, and iron and silicon isotope compositions of the soil solutions. Soil acronyms as in Fig. 1.

Soil horizon		Depth	pH$_{solution}$	Fe[a]	Si[a]	δ^{57}Fe	2 SD[b]	δ^{30}Si	2 SD
		cm		mg l^{-1}	mg l^{-1}	‰	‰	‰	‰
HA	A1	0-15	5.05	0.027	9.6	-0.23	0.10	0.37	0.13
HA	Bw1	26-40	4.67	0.023	9.6	-0.08	0.16	-0.19	0.07
HA	O1	57-67	3.99	0.032	24.2	-0.71	0.08	0.27	0.11
HA	redox	67-83	3.98	0.036	26.5	-0.28	*0.07*	0.12	0.02
HA	O2	83+	3.95	0.036	30.3	-1.36	0.08	-0.08	0.08
H	O1	0-13	4.88	0.282	10.5	-0.03	0.05	0.14	0.12
H	O2	13-26	5.47	0.059	5.3	0.38	*0.07*	0.15	0.13
H	O3	26-40	5.15	0.193	17.4	-	-	0.34	0.11
H	O4	52-63	-	15.250	19.2	-0.48	0.06	0.88	0.11
H	O5	63-72	-	-	-	-	-	-	-
H	O6	72+	-	19.980	18.8	0.14	0.03	1.22	0.16
BA	A1	0-21	-	0.012	5.9	-0.12	0.03	0.58	0.12
BA	A2	21-40	5.84	0.010	3.5	0.14	0.09	0.27	0.10
BA	Bw1	40-52	5.88	0.034	3.6	-0.01	0.07	-0.08	0.13
BA	Bw2	52-96	5.96	0.008	4.4	-	-	0.15	0.08
BA	Bw3/C	96+	5.46	0.004	5.0	-	-	-0.07	0.06
GA	A1	0-12	-	0.014	5.7	-	-	0.56	0.10
GA	A2	12-29	5.77	0.045	7.5	-	-	0.05	0.12
GA	Bw1	29-43	-	0.015	8.1	-	-	0.27	0.12
GA	Bw2	43-56	5.6	0.011	12.0	0.06	*0.07*	0.25	0.09
GA	2Bw1	64+	5.46	0.005	12.4	-	-	0.25	0.07

[a] data from Opfergelt et al., 2014; [b] in *italic* : for analyses where there was only enough Fe for one replicate, the 2SD of the in-house FeCl salt standard measured during the course of analysis is used

Table 3

Table 3. Main characteristics of river water samples: location, temperature, pH, conductivity, dissolved Fe concentration (<0.2µm), proportion of colloidal Fe (10kD-0.2µm) in the dissolved phase, iron isotope compositions of the dissolved and colloidal phases.

Sample name	Location	Latitude	Longitude	Temp.	pH	Conductivity	$[Fe]_{dissolved}$ (<0.2µm)	% Fe colloidal	$\delta^{57}Fe_{dissolved}$	2SD[a]	$\delta^{57}Fe_{colloid}$	2SD[a]
				°C		µS cm^{-1}	µg l^{-1}	(10kD-0.2µm)	‰	‰	‰	‰
A3	Grimsa	N64°35'57.6''	W21°34'75.3''	9.2	8.0	61	11.7	56	-0.30	0.03	-0.29	0.01
A4	Hvita (Ferjukot)	N64°36''19.9''	W21°42'48.1''	7.2	8.4	52	6.0	26	-0.46	*0.07*	-0.14	*0.07*
HA river	Hestur	N64°34'28.1''	W21°35'41.9''	-	-	-	6.7	-	-0.89	0.01	-	-

[a] in *italic* : for analyses where there was only enough Fe for 1 replicate, the 2SD of the in-house FeCl salt standard measured during the course of analysis is used
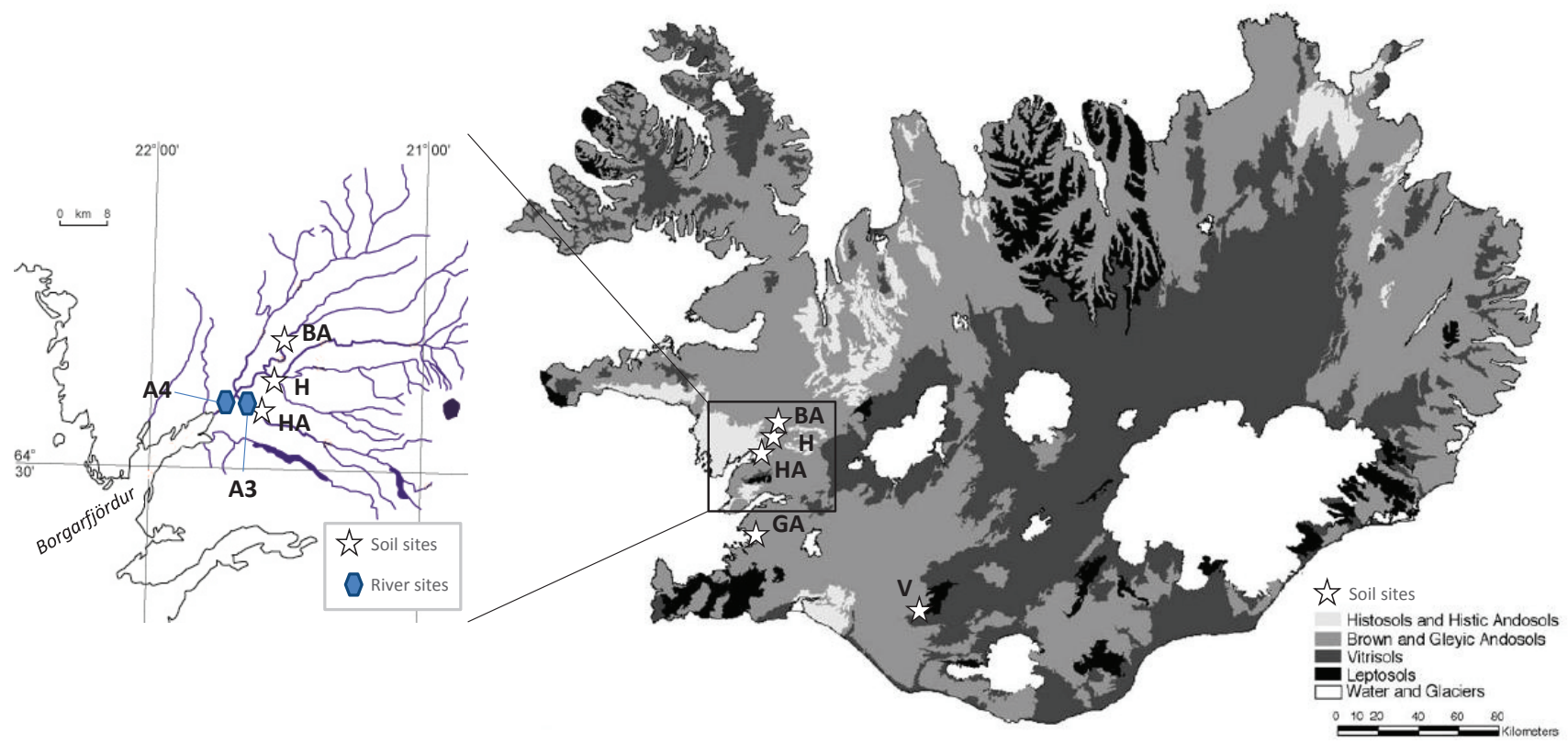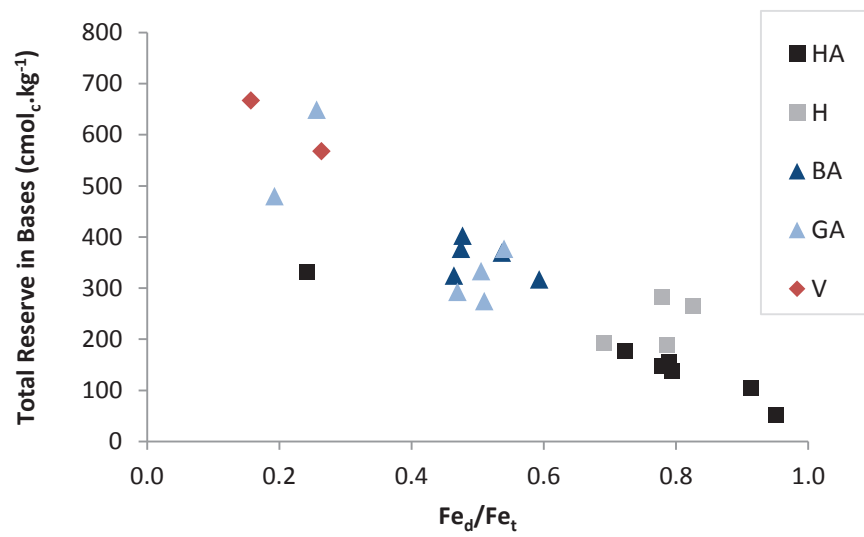
Figure 1

Figure 1.

Figure 2

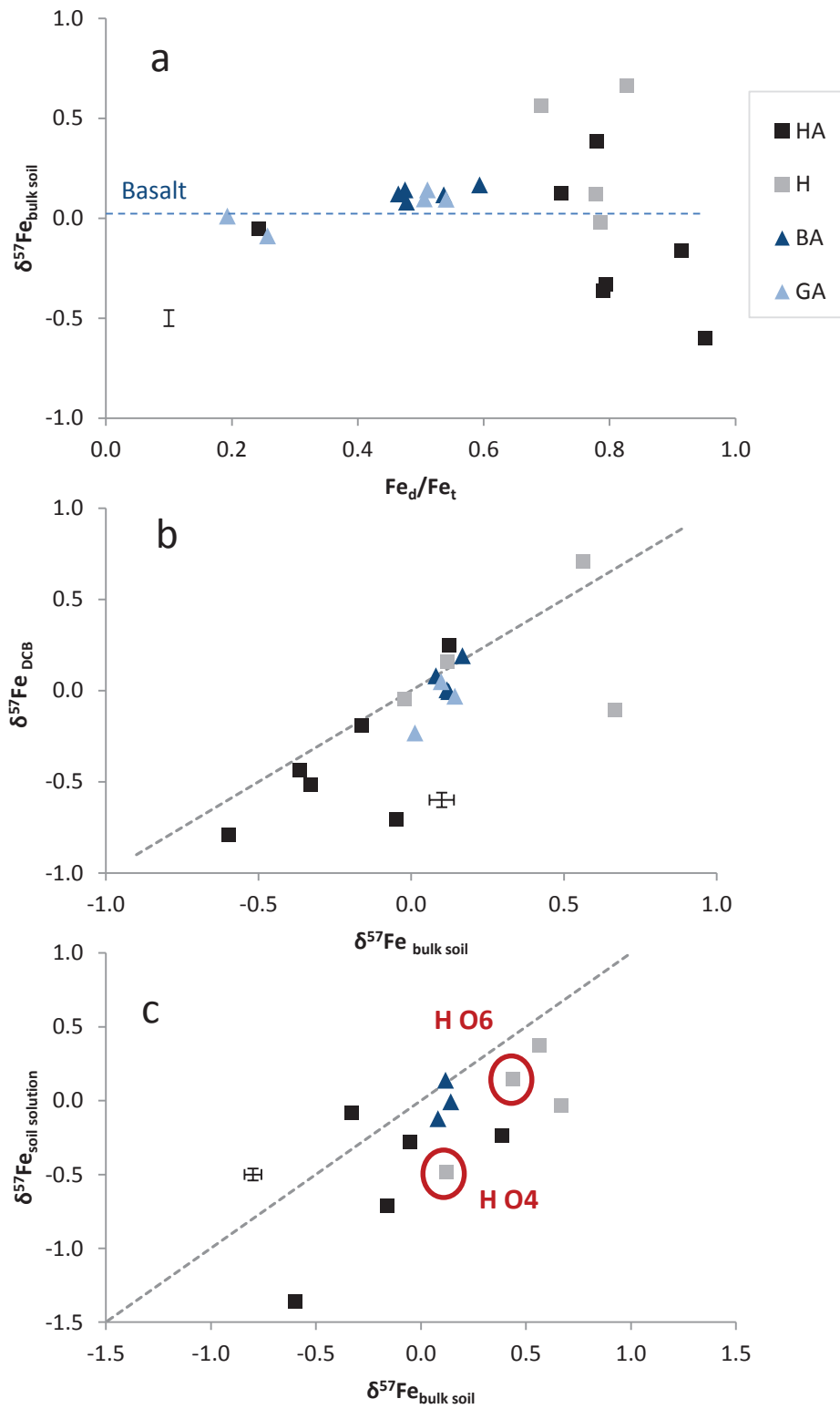**Figure 2.**

Figure 3

Figure 3.

Figure 4
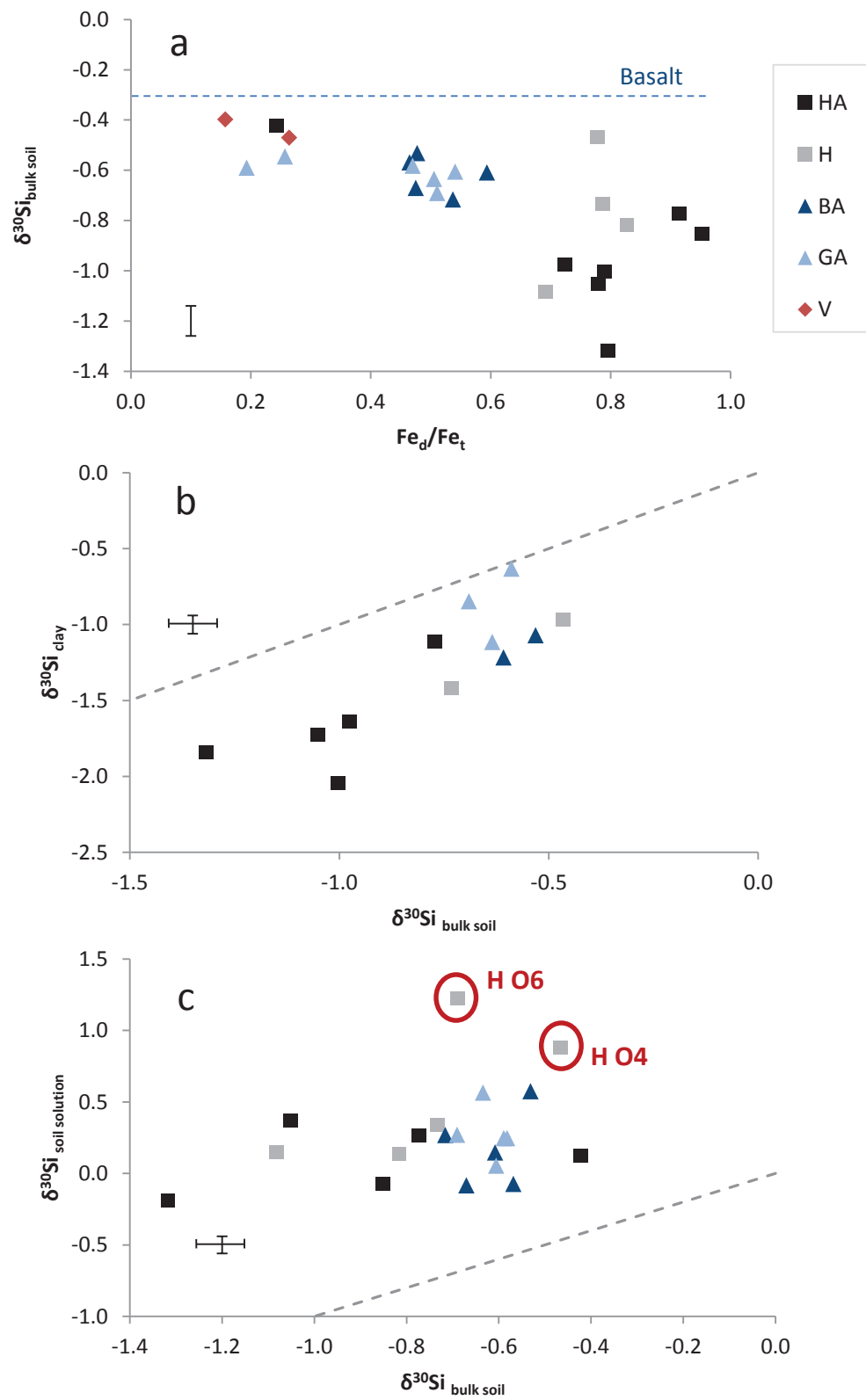
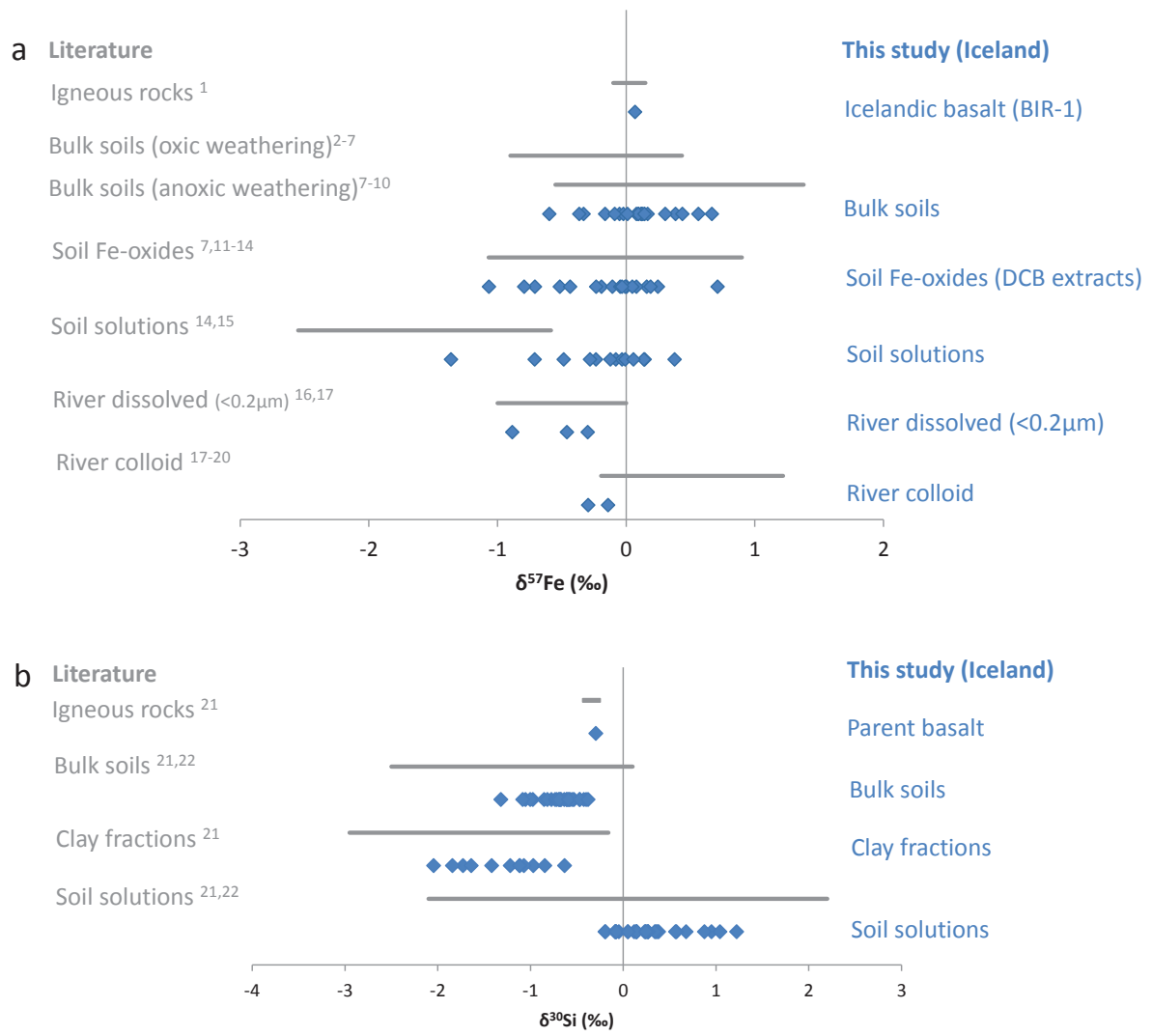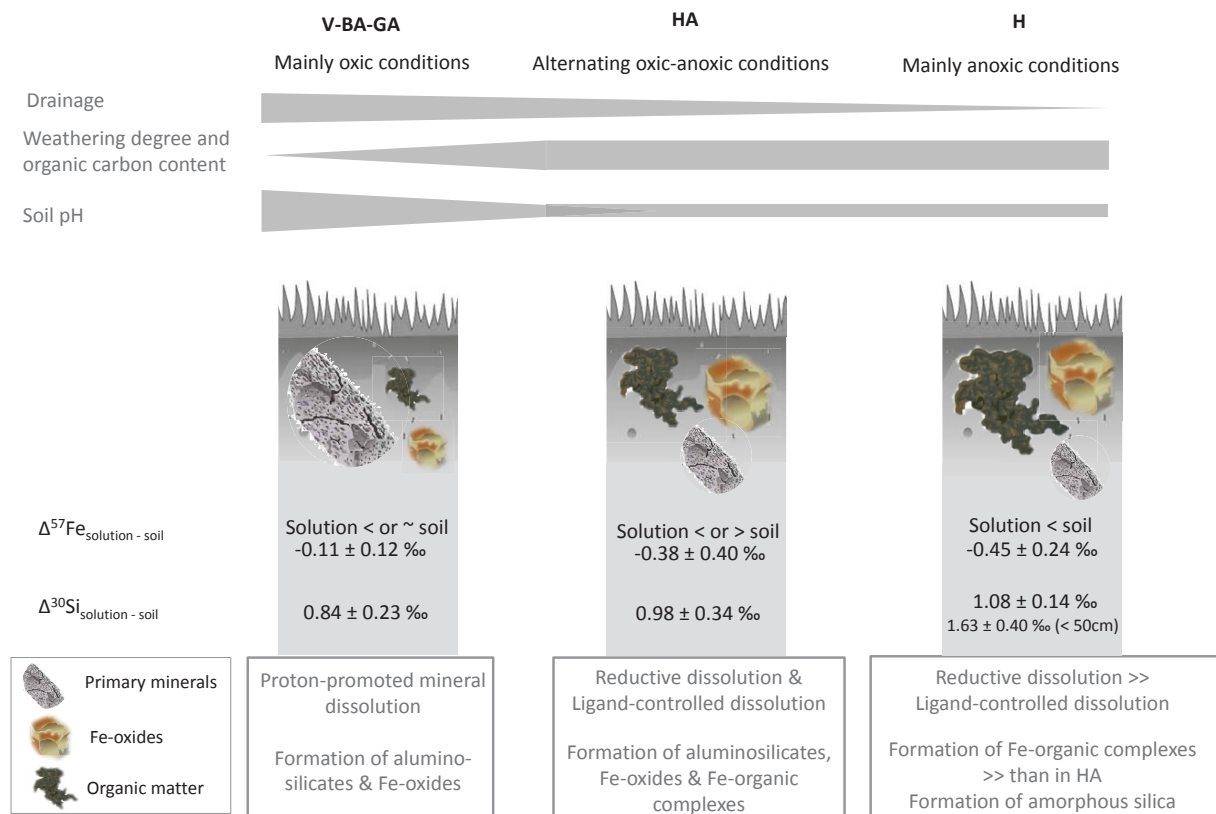**Figure 4.**

Figure 5

Figure 5.

Figure 6

	V-BA-GA	HA	H
	Mainly oxic conditions	Alternating oxic-anoxic conditions	Mainly anoxic conditions

Drainage

Weathering degree and organic carbon content

Soil pH

$\Delta^{57}Fe_{solution - soil}$

Solution < or ~ soil
-0.11 ± 0.12 ‰

Solution < or > soil
-0.38 ± 0.40 ‰

Solution < soil
-0.45 ± 0.24 ‰

$\Delta^{30}Si_{solution - soil}$

0.84 ± 0.23 ‰

0.98 ± 0.34 ‰

1.08 ± 0.14 ‰
1.63 ± 0.40 ‰ (< 50cm)

Primary minerals

Fe-oxides

Organic matter

Proton-promoted mineral dissolution

Formation of alumino-silicates & Fe-oxides

Reductive dissolution & Ligand-controlled dissolution

Formation of aluminosilicates, Fe-oxides & Fe-organic complexes

Reductive dissolution >> Ligand-controlled dissolution

Formation of Fe-organic complexes >> than in HA
Formation of amorphous silica

Figure 6.